Sr, Nd, Pb and trace element systematics of the New Caledonia harzburgites: Tracking source depletion and contamination processes in a SSZ setting

Arianna Secchiari, Alessandra Montanini, Delphine Bosch, Patrizia Macera, Dominique Cluzel

Geoscience Frontiers 11 (2020) 37–55

HOSTED BY

Contents lists available at ScienceDirect

China University of Geosciences (Beijing)

Geoscience Frontiers

journal homepage: www.elsevier.com/locate/gsf

Research Paper

Sr, Nd, Pb and trace element systematics of the New Caledonia harzburgites: Tracking source depletion and contamination processes in a SSZ setting

Arianna Secchiari [a], Alessandra Montanini [a,*], Delphine Bosch [b], Patrizia Macera [c], Dominique Cluzel [d]

[a] Dipartimento di Scienze Chimiche, della Vita e della Sostenibilità Ambientale, Università di Parma, Italy
[b] Geosciences Montpellier, Université de Montpellier, France
[c] Dipartimento di Scienze della Terra, Università di Pisa, Italy
[d] Institut des Sciences Exactes et Appliquées, Université de la Nouvelle-Calédonie, New Caledonia

ARTICLE INFO

Article history:
Received 26 October 2018
Received in revised form
2 February 2019
Accepted 2 April 2019
Available online 4 May 2019

Keywords:
Intra-oceanic arcs
Depleted mantle sections
Fore-ac harzburgites
New Caledonia ophiolite
Sr-Nd-Pb isotopes
Subduction zones

ABSTRACT

The New Caledonia ophiolite (Peridotite Nappe) consists primarily of harzburgites, locally overlain by mafic-ultramafic cumulates, and minor spinel and plagioclase lherzolites. In this study, a comprehensive geochemical data set (major and trace element, Sr-Nd-Pb isotopes) has been obtained on a new set of fresh harzburgites in order to track the processes recorded by this mantle section and its evolution.

The studied harzburgites are low-strain tectonites showing porphyroclastic textures, locally grading into protomylonitic textures. They exhibit a refractory nature, as attested by the notable absence of primary clinopyroxene, very high Fo content of olivine (91–93 mol.%), high Mg# of orthopyroxene (0.91–0.93) and high Cr# of spinel (0.44–0.71). The harzburgites are characterised by remarkably low REE concentrations (<0.1 chondritic values) and display "U-shaped" profiles, with steeply sloping HREE (Dy_N/Yb_N = 0.07–0.16) and fractionated LREE-MREE segments (La_N/Sm_N = 2.1–8.3), in the range of modern fore-arc peridotites. Geochemical modelling shows that the HREE composition of the harzburgites can be reproduced by multi-stage melting including a first phase of melt depletion in dry conditions (15% fractional melting), followed by hydrous melting in a subduction zone setting (up to 15%–18%). However, melting models fail to explain the enrichments observed for some FME (i.e. Ba, Sr, Pb), LREE-MREE and Zr–Hf. These enrichments, coupled with the frequent occurrence of thin, undeformed films of Al_2O_3, and CaO-poor orthopyroxene (Al_2O_3 = 0.88–1.53 wt.%, CaO = 0.31–0.56 wt.%) and clinopyroxene with low Na_2O (0.03–0.16 wt.%), Al_2O_3 (0.66–1.35 wt.%) and TiO_2 (0.04–0.10 wt.%) contents, point to FME addition during fluid-assisted melting followed by late stage metasomatism most likely operated by subduction-related melts with a depleted trace element signature.

Nd isotopic ratios range from unradiogenic to radiogenic ($-0.80 \leq \varepsilon_{Nd_i} \leq +13.32$) and negatively correlate with Sr isotopes ($0.70257 \leq {}^{87}Sr/{}^{86}Sr \leq 0.70770$). Pb isotopes cover a wide range, trending from DMM toward enriched, sediment-like, compositions. We interpret the geochemical signature displayed by the New Caledonia harzburgites as reflecting the evolution of a highly depleted fore-arc mantle wedge variably modified by different fluid and melt inputs during Eocene subduction.

1. Introduction

Subduction zones, where oceanic lithosphere is recycled into the mantle and arc volcanism is generated, are major loci of mass transfer between the Earth's surface and interior. The study of forearc sequences hence provides an exceptional opportunity to investigate the processes occurring during plate convergence, from

* Corresponding author.
E-mail address: alessandra.montanini@unipr.it (A. Montanini).
Peer-review under responsibility of China University of Geosciences (Beijing).

https://doi.org/10.1016/j.gsf.2019.04.004

subduction initiation to arc maturity (Reagan et al., 2010; Ishizuka et al., 2011; Brounce et al., 2015).

Currently, our knowledge concerning subduction processes, as well as geochemical models of the mantle wedge, mostly derive from geochemical and isotopic data obtained on arc lavas, while studies on peridotites are remarkably scarce. This is mainly due to the difficulty of sampling forearc mantle in active subduction zones. Comprehensive studies on subduction-related peridotites are thus crucial in order to improve our knowledge on the sub-arc mantle, as well as to understand how subduction zones evolve through time. To this end, studies on mantle sections originated in forearc settings that can be found in many ophiolitic complexes may provide robust constraints (e.g. Bodinier and Godard, 2014).

The New Caledonia ophiolite hosts one of the largest and best preserved forearc mantle sections in the world, offering a unique insight into upper mantle processes. Mantle lithologies are dominated by harzburgites and are locally capped by a mafic-ultramafic sequence, which is thought to represent a crust-mantle transect built at the beginning of the Eocene subduction event (Marchesi et al., 2009; Pirard et al., 2013; Secchiari et al., 2018). To date however, only scarce geochemical information is available for the New Caledonia harzburgites, while isotopic data are completely missing. Recent geochemical studies highlighted that these rock-types recorded high melting degrees in supra-subduction zone environment, possibly followed by re-enrichment in the subduction system (Marchesi et al., 2009; Ulrich et al., 2010; Pirard et al., 2013). However, the details about the evolution and the processes registered by this mantle section still remain poorly known.

Here, we present a comprehensive petrographic and geochemical characterisation of the main harzburgite bodies from New Caledonia, with the aim to bridge these gaps in knowledge, investigating melt extraction history and late-stage metasomatic processes. To this purpose, major and trace element contents were analysed in minerals and bulk rocks for a new set of samples of spinel harzburgites. In order to avoid the effects of secondary hydration (during cooling) and weathering (after obduction), unserpentinized and unweathered samples have been carefully selected from natural outcrops throughout the island. In addition, Sr-Nd-Pb isotope data were obtained on bulk rocks, to unravel the geochemical signatures of the New Caledonia harzburgites in the context of mantle end-members and to track contamination processes in the subduction zone system.

2. Geological and petrological background

New Caledonia is a NW–SE elongated island located in the SW Pacific region between the New Hebrides Arc (Vanuatu)and the eastern margin of Australia (Fig. 1a).

The main island of New Caledonia is composed of an assemblage of volcanic, sedimentary and metamorphic terranes ranging in age from Permian to Miocene (Aitchison et al., 1995; Cluzel et al., 2001, 2012; Lagabrielle et al., 2013). These terranes were assembled during two tectonic events: a Permian to Early Cretaceous west-dipping subduction, related to the east Gondwana active margin, and an Eocene north-east dipping subduction that eventually resulted in obduction. Both tectonic events were marked by high-pressure (HP-LT) metamorphism, as attested by the metamorphic lithologies occurring in the Boghen terrane ("ante-Permien"; Paris, 1981) and in the Diahot and Pouebo terranes (Cluzel et al., 2012a, b). Peak metamorphic age is poorly constrained for the Boghen terrane (~150 Ma, based on whole rock K–Ar data for blueschists and metabasalts, see Blake et al., 1977), while an age of ~44 Ma for the Eocene metamorphism has been obtained by means of U–Pb zircon dating of eclogite facies rocks (Spandler et al., 2005).

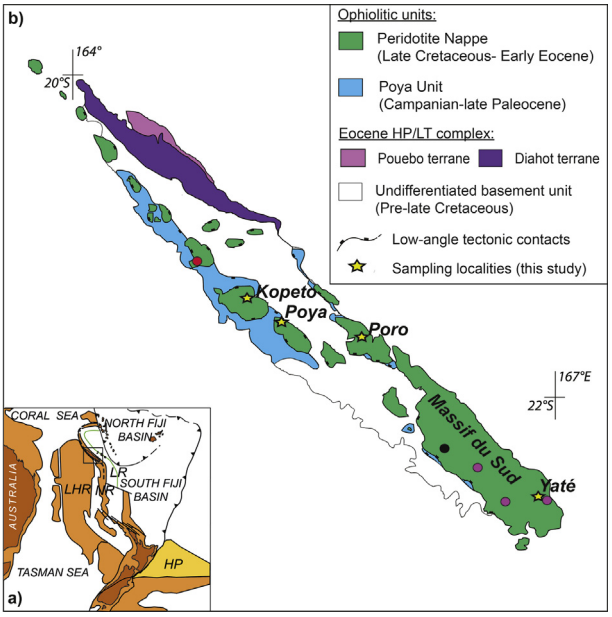

Fig. 1. (a) Present-day structures of the Southwest Pacific region. Dark orange, land; light orange, continental plateau; white, oceanic basins (LHR: Lord Howe Rise, NR: Norfolk ridge, LR: Loyalty ridge, HP: Hikurangi Plateau). (b) Simplified sketch map of New Caledonia showing the distribution of the Peridotite Nappe, Poya Terrane and autochtonous units. Yellow stars represent main sampling locations of this study: Kopeto, Poya, Poro, Yaté (see Table 1 for details); sampling localities of previous works are reported as black (Marchesi et al., 2009), red (Ulrich et al., 2010) and pink circles (Pirard et al., 2013).

Following Cluzel et al. (2001), the island can be divided into four main geological domains: (i) the autochtonous units, including a pre-late Cretaceous basement and its Late Coniacian-to-late Eocene sedimentary cover, (ii) the Eocene HP-LT metamorphic belt, (iii) the dominantly basaltic Poya Terrane and (iv) a large sheet of obducted mantle rocks referred as the Peridotite Nappe (Avias, 1967).

The Peridotite Nappe represents the obducted oceanic lithosphere of the Loyalty Basin (Collot et al., 1987), which recorded a marginal basin formation followed by Eocene convergence and obduction in a NE-dipping subduction zone (Cluzel et al.,1998).

The Peridotite Nappe constitutes one of the largest mantle exposure worldwide and a major feature of the New Caledonia geology, covering approximately 8000 km^2. The spatial distribution of this terrane includes several tectonic klippen spread along the west coast, some smaller lenses in the central chain and a larger unit named "Massif du Sud", which dominates the southern part of the island. The Peridotite Nappe reaches a maximum thickness of ~2500 m and is bounded at the bottom by a highly-sheared serpentinite sole related to the thrust fault responsible for the obduction. Kinematic indicators of the serpentinite sole indicate top to the SW thrusting (Quesnel et al., 2016).

With the exception of the northernmost lherzolitic massifs, the Peridotite Nappe is dominated by harzburgite tectonites, locally overlain by a sequence of dunites, wehrlites, rare pyroxenites and gabbroic rocks, interpreted as a crust-mantle transect originated in a nascent arc environment. The formation of this sequence has been ascribed to migration and accumulation in the upper mantle-lower crust transition of primitive ultra-depleted magma batches (Marchesi et al., 2009; Pirard et al., 2013; Secchiari et al., 2018).

Notably, the upper oceanic crust is completely absent in the ophiolite (Prinzhofer et al., 1980; Prinzhofer and Allègre, 1985). According to Cluzel et al. (2001) the crustal sequence was most likely eroded or tectonically detached before, during and/or after obduction. Basaltic rocks with contrasting geochemical signatures,

ranging from back-arc basin basalts (BABB) to E-MORB compositions (e.g. Cluzel et al., 2001), occur in the Poya Terrane, which tectonically underlies the Peridotite Nappe. The age and the origin of the Poya Terrane and its possible genetic link with the Peridotitic Nappe are still a matter of debate (Eissen et al., 1998; Ulrich et al., 2010; Secchiari et al., 2016). Geochronological constraints for the Poya terrane are limited to few K–Ar data, indicating significantly lower ages (~38–49 Ma; Eissen et al., 1998) than those provided by the palaeontological record of the sedimentary rocks closely associated with the Poya volcanics (i.e. Campanian-late Paleocene; Cluzel et al., 2001). The radiometric ages of the basalts are thought to reflect resetting due to the emplacement and subsequent metamorphism beneath the overriding harzburgite nappe (Cluzel et al., 2001).

Boudins of clinoenstatite-bearing boninites of lower Eocene age have been found within the serpentine myloniteat the base of the Peridotite Nappe (Cluzel et al., 2012a, 2016). The origin of the boninites has been recently attributed by Cluzel et al. (2016) to hydrous melting of a depleted mantle source re-enriched by slab melts.

The Peridotite Nappe is crosscut at all levels by doleritic basalts with IAT (Island Arc Tholeiitic) affinity, microdiorites and granitoid ("adakite-like") dykes, which are not present in the underlying Poya Terrane. According to U–Pb zircon dating, the felsic dykes were emplaced within a narrow time span (55–50 Ma; Cluzel et al., 2006), which is thought to represent the beginning of magmatic activity in the subduction system, as well as the minimum age constraint for the oceanic lithosphere formation.

The New Caledonia harzburgites are ultra-depleted rock-types, as testified by the lack of primary clinopyroxene and the notably low trace element contents (Prinzhofer and Allègre, 1985; Marchesi et al., 2009). For this reason, their origin and evolution have remained unclear for long time, due to the analytical difficulties of reaching an adequate geochemical characterisation. However, three decades after the first pioneering studies (Prinzhofer et al., 1980; Dupuy et al., 1981; Prinzhofer and Allègre, 1985), a renewed phase of interest for the ophiolite has led to the publication of new works, with a significant improvement in our knowledge of these mantle rocks.

Recent geochemical studies (Marchesi et al., 2009; Ulrich et al., 2010; Pirard et al., 2013) have converged on the consensus that the New Caledonia harzburgites have a supra-subduction affinity closely linked to the Eocene subduction event. Geochemical modelling showed that the depleted compositions of the harzburgites can be reproduced by high amount of partial melting (up to 25%; e.g. Marchesi et al., 2009; Ulrich et al., 2010).

By contrast, slightly depleted spinel and plagioclase lherzolites, similar to modern abyssal-type peridotites, occur in the northern part of the island (Ulrich et al., 2010; Secchiari et al., 2016). The main geochemical and petrological features of these rock-types are thought to reflect moderate partial melting degrees (8%–9%) in a MOR environment, followed by low-pressure refertilization by non-aggregated MORB-type melts, giving rise to plagioclase lherzolites. Geochemical and isotopic data seem to preclude an involvement of these lithologies in the Eocene subduction system (Secchiari et al., 2016). However, a possible genetic link between the New Caledonia lherzolites and harzburgites remains difficult to establish based on the available data.

3. Analytical methods

Major element mineral analyses were performed at Chemistry, Life Sciences and Environmental Sustainability Department in Parma using a JEOL-6400 electron microprobe equipped with a LINK-ISIS energy dispersive microanalytical system. The electron beam was produced at an accelerating voltage of 15 kV and probe current of 0.25 nA; both natural minerals and synthetic compounds were used as standards.

Samples for bulk rock analyses were sawn into thin slabs and altered parts were carefully removed before crushing. In order to obtain representative major and trace element analyses, rock samples were prepared from at least 1 kg of material and crushed to powder in agate mill. Whole-rock major oxides and Ni, Co, Cr, V, Zn were measured by conventional XRF techniques at the Department of Chemical and Geological Sciences in Modena using a wavelength dispersive X-ray fluorescence spectrometer (Philips PW 1480).

Whole-rock and in situ trace element analyses were performed at the AETE-ISO technical platform ("Trace Element Analysis in the Environment and ISOtopes", Université de Montpellier). Bulk trace element concentrations (excluding Ni, Co, Cr, V, Zn) were determined using a ThermoFinnigan ELEMENT XR (HR-ICP-MS: high resolution inductively coupled plasma mass spectrometer) after acid digestion with HNO_3-HF-$HClO_4$, as described by Ionov et al. (1992).

Trace element compositions of orthopyroxene were measured in-situ on polished thick sections by ThermoFinnigan ELEMENT XR high resolution (HR) ICP-MS coupled with a Geolas Lambda Physik CompEx 102 EXCIMER. Signals were acquired in Time Resolved Acquisition, devoting 2 min for the blank and 1 min for measurement of the analytes. The laser was fired employing an energy density of 15 J/cm^2 at a frequency of 8–10 Hz and using a spot size of 102 μm. Reference sample BIR-1G was analyzed as unknown during the analytical runs and shows good agreement with working values for this international standard. Si was used as internal standard and analyte concentrations were calibrated against the NIST 612 rhyolitic glass, according to the values of Pearce et al. (1997). Data were subsequently reduced using the GLITTER software by inspecting the time-resolved analysis and selecting time intervals in which signal intensities were homogeneous.

Sr-Nd-Pb isotopes were analysed on 6 whole rock samples and 2 duplicates. Powdered samples were weighted to obtain approximately 50 to 200 ng of Sr, Nd and Pb. A leaching step with 6 N HCl during 60 min at 95 °C was done before acid digestion. After leaching, residues were rinsed three times in purified Milli-Q H_2O. Samples were subsequently dissolved during 72 h on a hot plate with a mixture of HF and HNO_3 (1:1). After evaporation to dryness, 2 mL of HNO_3 was added to the residue and kept at 95 °C for 24–48 h.

Strontium isotopes were separated using Sr Eichrom resin (Pin et al., 1994), while Neodymium isotopes were extracted in two steps, a first using AG50WX12 cationic exchange resin followed by a second to purify REE using HDEHP conditioned Teflon columns.

For Pb separation, after complete evaporation, 0.05 mL of 8 N HBr was added to the sample and kept at 70 °C for 2–3 h before another complete evaporation. The chemical separation of Pb was done using anion exchange resin (AG1X8, 200–400 mesh) with samples being loaded and washed in 0.5 N HBr. Lead was then eluted in 6 N HCl.

Sr isotopic ratios were measured by thermal ionization mass spectrometry using a Triton Finnigan Mat spectrometer from the Labogis in Nîmes University. $^{87}Sr/^{86}Sr$ isotopic ratios were normalised using a value of 0.1194 for the $^{86}Sr/^{88}Sr$ ratio. NBS987 standards have been analyzed during the course of this study and yield an averaged $^{87}Sr/^{86}Sr$ ratio of 0.710258 ± 4.

Nd and Pb isotopic analyses were performed using a Nu 500 HR MC-ICP-MS at the "Service Commun National d'Analyse" from the Ecole Normale Supérieure (ENS, Lyon, France). The standard average values were 0.511902 ± 5 (2σ) for the AMES-Rennes Nd standard (Chauvel and Blichert-Toft, 2001). NBS981 Pb standards were analysed in bracketing every two samples and yielded a

reproducibility better than 60 ppm for the three Pb/Pb ratios used, i.e. $^{206}Pb/^{204}Pb$, $^{207}Pb/^{204}Pb$, $^{208}Pb/^{204}Pb$.

4. Results

4.1. Petrography and mineralogy

For this work, nine samples of harzburgites have been selected. The samples were collected from four different areas: Kopeto, Poro, Poya and Yaté (see Fig. 1 and Table 1).

In the field, the harzburgites show a well-developed tectonitic structure (Fig. 2a), in which foliation and lineation can be determined from orthopyroxene porphyroclasts orientation (Pirard et al., 2013). They also locally occur as massive bodies (Fig. 2b and c).

From a petrographic point of view, the studied harzburgites are low-strain tectonites showing dominant porphyroclastic textures (Fig. 3a), locally grading into proto-mylonite. Recrystallised domains bearing equigranular mosaic-type textures are commonly found in all the analysed samples (Fig. 3b). A protogranular texture has been observed only for the sample YA1.

In the harzburgites the main mineral assemblage consists of olivine (~75–85 vol.%), orthopyroxene (~15–25 vol.%) and spinel (≤1 vol.%), while primary clinopyroxene is remarkably absent.

Table 1
Whole-rock major (wt.%) and trace element (ppm) compositions of the New Caledonia harzburgites. Trace element were determined by ICP-MS, with the exception of Ni, Co, Cr, V, Zn, which were measured by conventional XRF techniques.
LOI: loss on ignition; Mg# = 100 × cationic Mg/(Mg + Fe) with all the Fe as Fe^{2+}; bdl = below detection limit.

Location	Kopeto	Kopeto	Kopeto	Kopeto	Kopeto	Poro	Poro	Poya	Yaté
Sample	KPT1	KPT2	KPT3	KPT4	KPT5	PO3	PO4	PY1	YA1
Rock type	Harz	Harz	Harz	Sp harz	Sp harz	Sp harz	Sp harz	Sp harz	Sp harz
Lat. (°S)	21°11′50.95″	21°11′50.95″	21°11′50.95″	21°11′50.95″	21°11′50.95″	21°18′32.3″	21°17′49.8″	21°22′50.25″	22°09′25.2″
Long. (°E)	165°04′31.45″	165°04′31.45″	165°04′31.45″	165°04′31.45″	165°04′31.45″	165°41′48.2″	165°43′37.31″	165°16′22.94″	166°49′07.8″
Major elements									
SiO_2	45.08	43.71	44.03	44.10	43.64	43.62	43.77	43.65	41.05
Al_2O_3	0.72	0.70	0.67	1.21	0.74	0.41	0.43	0.78	0.46
FeO^t	7.16	6.86	7.39	7.22	7.02	7.15	6.95	7.43	6.37
MnO	0.12	0.11	0.12	0.12	0.12	0.12	0.11	0.12	0.10
MgO	45.47	44.37	45.77	45.74	47.06	47.62	47.44	46.66	44.16
CaO	0.66	0.46	0.53	0.59	0.52	0.29	0.35	0.54	0.31
Na_2O	bdl	bdl	bdl	bdl	bdl	bdl	bdl	bdl	bdl
K_2O	bdl	bdl	bdl	bdl	bdl	bdl	bdl	bdl	bdl
TiO_2	bdl	0.01	0.01	bdl	0.01	0.01	0.01	0.01	0.01
P_2O_5	bdl	bdl	bdl	bdl	bdl	bdl	bdl	bdl	bdl
LOI	bdl	3.03	0.67	0.22	0.12	bdl	0.18	bdl	6.83
Total	99.21	99.25	99.19	99.20	99.23	99.22	99.24	99.19	99.29
Mg#	91.89	92.03	91.71	91.88	92.29	92.24	92.41	91.81	92.52
Trace elements									
Cr	3016	2763	2845	2707	2836	2795	2791	2879	1913
V	26	29	30	28	24	22	25	26	18
Ni	2418	2422	2441	2496	2488	2523	2544	2486	2282
Co	141	138	141	143	136	145	145	143	134
Zn	43	48	46	46	54	47	46	50	42
Rb	0.02	0.02	0.03	0.01	0.02	0.03	0.02	0.02	0.02
Sr	0.14	0.22	0.20	0.14	0.22	0.10	0.17	0.35	0.45
Y	0.01	0.01	0.01	0.01	0.05	bdl	0.02	0.02	0.04
Zr	0.02	0.03	0.06	0.03	0.13	0.12	0.02	0.02	0.05
Nb	0.005	0.005	0.006	0.005	0.014	0.004	0.006	0.005	0.004
Cs	0.001	0.005	0.002	0.001	0.001	0.001	0.001	0.001	0.001
Ba	0.10	0.28	0.30	0.12	0.41	0.23	0.42	0.28	0.32
La	0.002	0.006	0.012	0.002	0.014	0.005	0.003	0.004	0.005
Ce	0.003	0.012	0.024	0.005	0.026	0.006	0.003	0.005	0.011
Pr	bdl	0.001	0.002	0.001	0.003	0.001	0.001	0.001	0.002
Nd	0.002	0.003	0.007	0.002	0.017	0.003	0.003	0.002	0.010
Sm	bdl	0.001	0.001	0.001	0.004	0.001	0.001	bdl	0.002
Eu	bdl	bdl	bdl	bdl	0.002	bdl	bdl	0.002	0.001
Gd	0.001	0.001	0.001	0.001	0.006	0.001	0.001	0.001	0.003
Tb	bdl	bdl	bdl	bdl	0.001	bdl	bdl	bdl	0.001
Dy	0.001	0.001	0.001	0.001	0.007	0.001	0.002	0.001	0.006
Ho	bdl	bdl	bdl	bdl	0.002	bdl	0.001	bdl	0.001
Er	0.001	0.002	0.002	0.002	0.005	0.001	0.002	0.003	0.005
Tm	0.001	0.001	0.001	bdl	0.001	bdl	0.001	0.001	0.001
Yb	0.006	0.007	0.007	0.006	0.010	0.003	0.007	0.010	0.008
Lu	0.001	0.002	0.002	0.002	0.002	0.001	0.002	0.003	0.002
Hf	0.001	0.001	0.002	0.001	0.004	0.003	0.001	0.001	0.002
Pb	0.27	0.39	0.26	0.31	0.22	0.27	0.25	0.71	0.32
Th	0.001	0.002	0.001	0.002	0.002	0.001	0.001	0.001	0.001
U	bdl	bdl	bdl	bdl	0.001	bdl	bdl	bdl	bdl
Dy_N/Yb_N	0.08	0.11	0.11	0.14	0.51	0.12	0.16	0.07	0.50
La_N/Sm_N	3.22	5.44	8.30	2.22	2.13	5.46	2.82	6.07	1.29
Sm_N/Dy_N	1.11	1.10	1.31	0.87	0.99	1.94	0.72	0.65	0.71

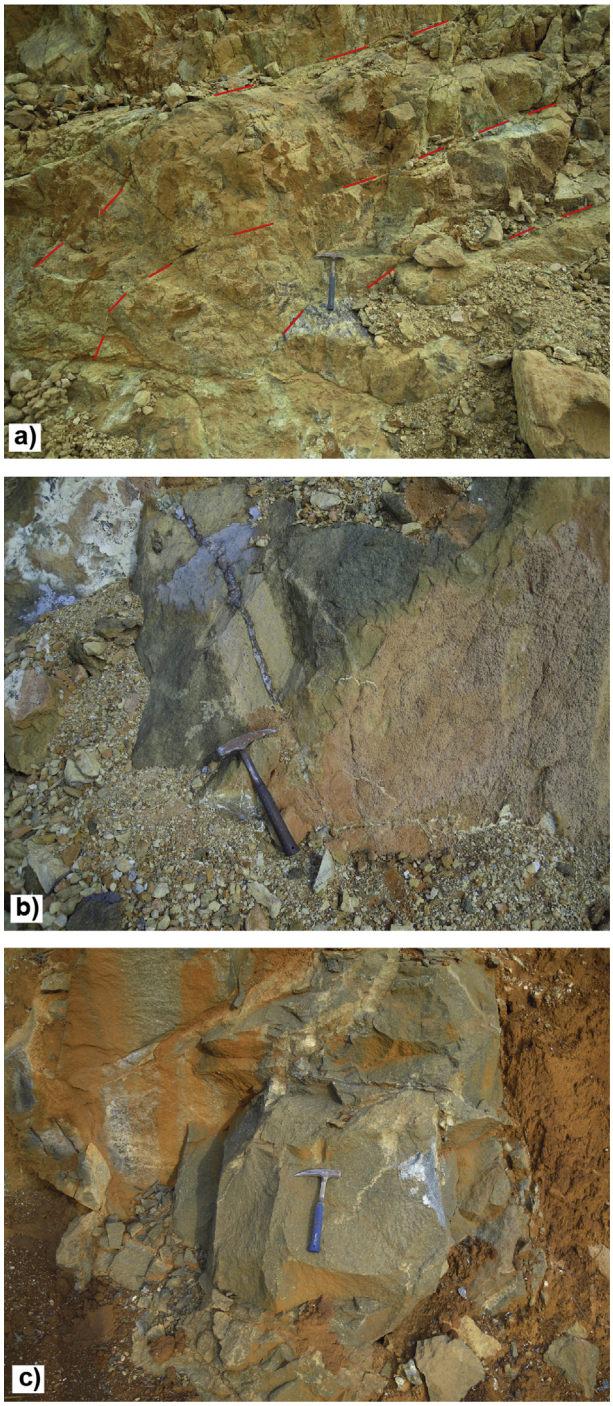

Fig. 2. Different appearance of the New Caledonia harzburgites in the field: (a) fresh harzburgite body from Kopeto mine; fracturation surfaces (red lines) follow the former tectonitic foliation (see also Fig. 3a); (b) massive harzburgite including dunite layers (Poro mine); (c) altered harzburgite outcrop in the Yaté area. Hammer length is about 30 cm.

Olivine occurs as elongated and kinked porphyroclasts (Fig. 3a), defining a foliation together with orthopyroxene and spinel. Olivineis characterised by high Mg# ranging from 0.908 to 0.933 and NiO content varying between 0.24 wt.% and 0.72 wt.%.

Coarse-grained (up to 2 mm in size) orthopyroxene porphyroclasts (Fig. 3c) show evidence of ductile deformation (undulous extinction and kink bands) and exsolution lamellae of clinopyroxene. They frequently display irregular outlines and embayments filled with fresh, undeformed olivine crystals (Fig. 3d). Olivine and orthopyroxene porphyroclasts are surrounded by domains consisting of polygonal or irregularly shaped neoblasts of the same phases (e.g. Fig. 3c).

Primary orthopyroxene is enstatitic in composition (see Supplementary Table S1) and shows Mg# falling between 0.914 and 0.924. Al_2O_3 and Cr_2O_3 cover the range of 1.30–2.73 wt.% and 0.60–1.12 wt.%, respectively, with decreasing values from core to rim. CaO contents of porphyroclast cores varies between 0.90 wt.% and 1.49 wt.%. As a whole, recrystallized orthopyroxene is characterised by comparable Mg#, Al_2O_3 and Cr_2O_3, associated with lower CaO contents (0.62–1.05 wt.%).

Small crystals of secondary, exsolution-free and undeformed orthopyroxene with interstitial habit are frequently observed (Fig. 3e). Secondary orthopyroxene has remarkably low Al_2O_3 (0.88–1.53 wt.%), Cr_2O_3 (0.32–0.88 wt.%) and CaO (0.31–0.56 wt.%) concentrations.

In addition, small clinopyroxene crystals have been detected as secondary phase in some of the studied samples (KPT1, KPT5, PO3, PY1, YA1). Clinopyroxene occurs as rounded grains ($\simeq$ 100 μm) in association with secondary interstitial orthopyroxene or thin films around olivine porphyroclasts (Fig. 3e). Clinopyroxene displays notably high Mg# values (0.943–0.952), coupled with low Al_2O_3, Cr_2O_3 and FeO contents (0.66–1.35 wt.%, 0.33–0.67 wt.% and 1.70–1.98 wt.%, respectively). Na_2O (0.03–0.16 wt.%) and TiO_2 (<0.10 wt.%) concentrations are also very low (see Supplementary Table S1).

Chromian spinel occurs as reddish-dark brown crystals, showing rounded or holly leaf shape. Symplectitic intergrowths with orthopyroxene (Fig. 3f) are often observed in some harzburgite samples (KPT1, KPT3, KPT4, and YA1). These structures are commonly found in peridotitic rocks, where they have been interpreted as derived from garnet breakdown (Morishita and Arai, 2003) or from melt-rock reactions (Seyler et al., 2007).

Spinel composition is homogeneous within each sample but displays some variability among harzburgites from the different localities. Al_2O_3 varies between 15.23 wt.% and 33.23 wt.% and shows core-to-rim increasing values. It is negatively correlated with Cr_2O_3 (38.57–57.57 wt.%), which in turns displays lower concentrations moving from porphyroclast cores to rims. Spinel Cr# and Mg# are remarkably high, ranging between 0.441–0.714 and 0.474–0.704, respectively (see Supplementary Table S1). These compositions overlap with the field of the supra-subduction zone peridotites (Fig. 4a) defined by Dick and Bullen (1984) and Arai (1994), in contrast with the lower Mg# and Cr# recorded by the New Caledonia spinel lherzolites (Secchiari et al., 2016). However, some samples from Kopeto, Poya and Yaté straddle the field of supra-subduction zone and abyssal-type peridotites. A similar distribution is also described in the olivine Mg# vs. spinel Cr# diagram (see Fig. 4b).

Secondary phases in the studied lithologies include chlorite, rare serpentine (YA1) and minute crystals of colourless amphibole, often in association with talc. Amphibole occurs as single acicular crystals crosscutting the main mantle paragenesis and/or the neoblastic assemblages (Fig. 3b) or form fibrous aggregates around olivine and orthopyroxene porphyroclasts (Fig. 3g). Clinopyroxenes are characterised by high Mg# (0.940–0.965), low Al_2O_3, Cr_2O_3 and Na_2O contents (Al_2O_3 = 0.94–2.15 wt.%, Cr_2O_3 = 0.20–0.81 wt.%, Na_2O = 0.02–0.51 wt.%, see Supplementary Table S1) and can be classified as tremolite according to the nomenclature of Hawthorne et al. (2012).

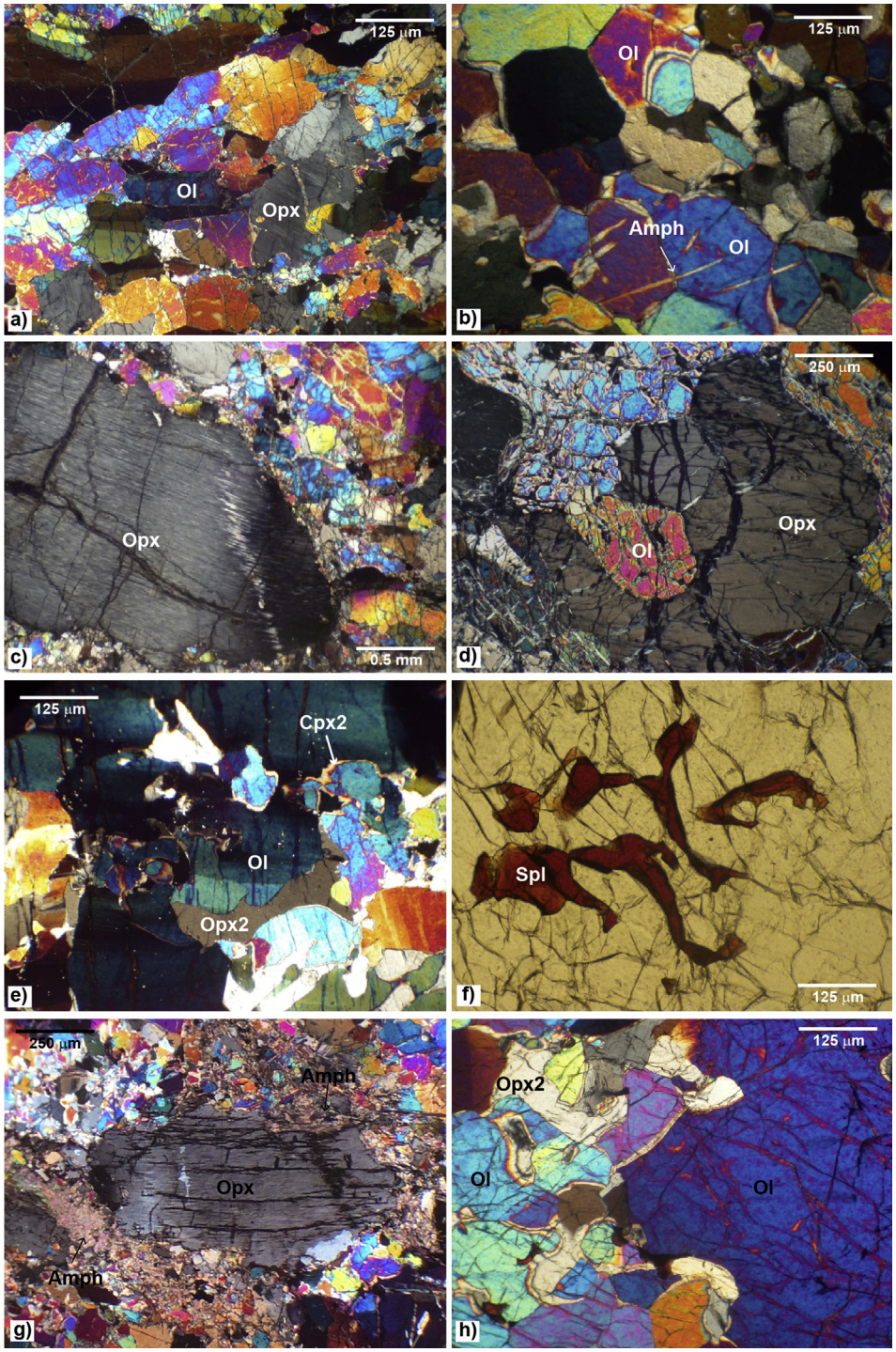

Fig. 3. (a) Kinked olivine porphyroclasts with preferred shape orientation in foliated tectonite (KPT1); (b) olivine and orthopyroxene neoblasts forming mosaic structure aggregates (PY1); (c) strongly deformed orthopyroxene porphyroclast in olivine + orthopyroxene + spinel matrix (KPT2); (d) orthopyroxene embayment filled with fresh and undeformed olivine (YA1); (e) interstitial films of clinopyroxene along olivine porphyroclasts boundaries (KPT5); (f) spinel-clinopyroxene-orthopyroxene symplectites (KPT3); (g) tremolitic amphibole development on orthopyroxene porphyroclasts (PY1); (h) secondary, interstitial orthopyroxene formed at the expense of porphyroclastic olivine (KPT1). Abbreviations: Ol, olivine; Opx, orthopyroxene; Amph, amphibole; Opx2, secondary orthopyroxene; Cpx2, secondary clinopyroxene; Spl, spinel.

4.2. Whole rock major and trace element composition

Major and trace element compositions of the New Caledonia harzburgites are listed in Table 1 and plotted in Figs. 5 and 6a, b.

The studied harzburgites are extremely fresh lithotypes (LOI $\leq$ 3 wt.%), with the exception of the sample YA1, which exhibits a higher serpentinisation degree (LOI = 6.8 wt.%).

The harzburgites possess high Mg# values (91.7–92.5) and low to very low contents of fusible elements, as Al_2O_3 (0.41–1.21 wt.%), CaO (0.29–0.66 wt.%) and TiO_2 ($\leq$0.01 wt.%), in the range of the harzburgites from Izu-Bonin-Mariana forearc (Parkinson and Pearce, 1998; Zanetti et al., 2006). MgO ranges between 44.16 wt.% and 47.62 wt.% and is negatively correlated with SiO_2 (41.05–45.08 wt.%), and Al_2O_3 (Fig. 5), as expected from mantle melting.

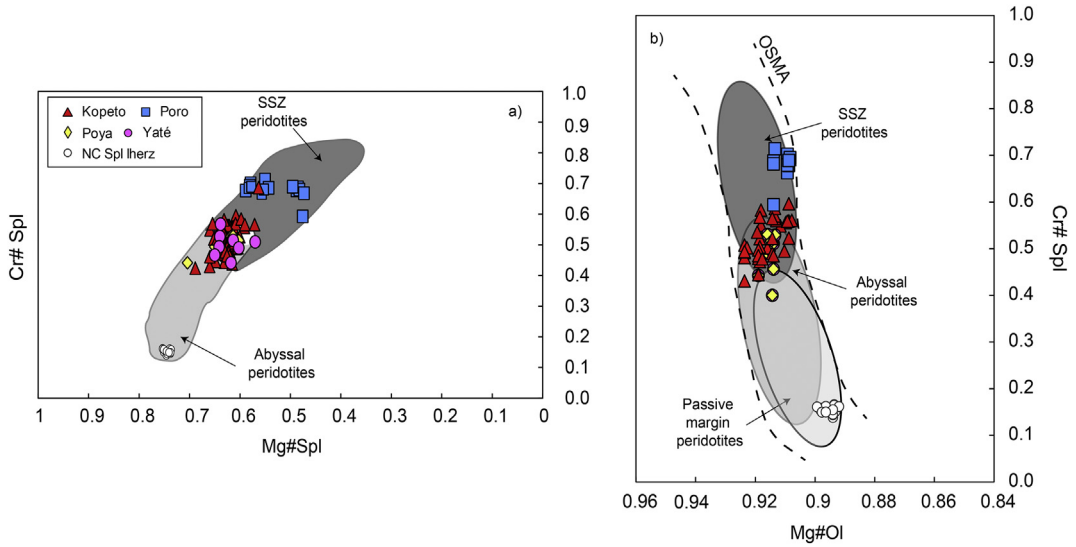

Fig. 4. Compositional variations of spinel: (a) Cr# vs. Mg#. Field for abyssal and forearc peridotites are from Dick and Bullen (1984) and Ishii et al. (1992), respectively; (b) average olivine Mg# and spinel Cr# for the New Caledonia harzburgites. The olivine–spinel mantle array (OSMA) is shown by dashed lines. Field for suprasubduction zone, abyssal and passive margins peridotites are after Dick and Bullen (1984), Arai (1994) and Pearce et al. (2000). Data for the New Caledonia spinel lherzolites are from Secchiari et al. (2016).

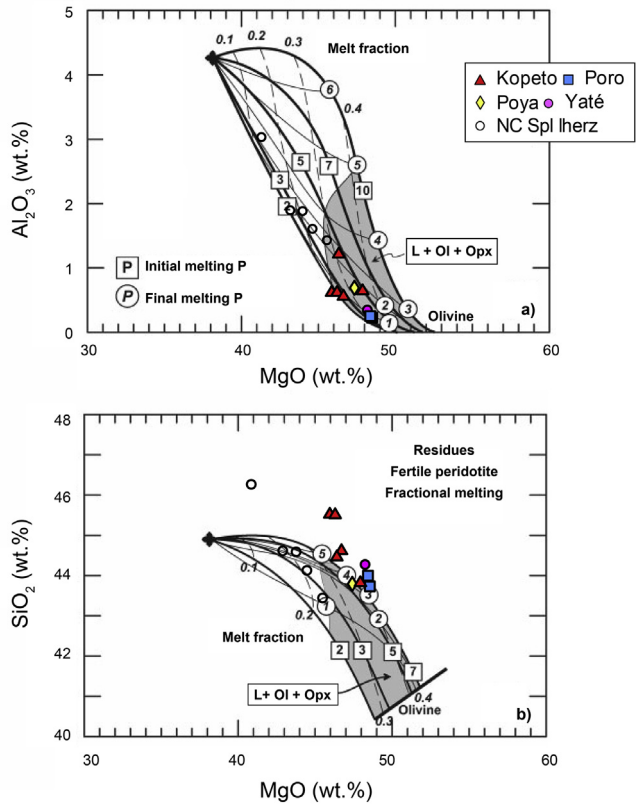

Fig. 5. Whole rock abundances of Al_2O_3 and SiO_2 vs. MgO (data on anhydrous basis in wt.%) for the New Caledonia harzburgites compared with model trends for residual peridotites after Herzberg (2004). Gray shaded fields are compositions of residual harzburgite designated as L + Ol + Opx. Light shaded fields bounded by the field of harzburgite residues and the bulk composition (bold cross) represent various spinel or garnet peridotite assemblages. Bold lines labelled with squares, initial melting pressures in GPa; light lines labelled with circles, final melting pressures; light dashed lines, melt fractions. Modified after Herzberg (2004). Data for the New Caledonia spinel lherzolites (Secchiari et al., 2016) are also shown for comparison.

Chondrite-normalised rare earth element (REE) patterns of the New Caledonia harzburgites are illustrated in Fig. 6a. All the samples display exceedingly low REE contents, with concentrations ranging between 0.002 and 0.1 times chondritic abundances. The harzburgites are characterised by "U-shaped" profiles, with steeply plunging HREE ($Dy_N/Yb_N = 0.07–0.16$) and fractionated LREE-MREE segments ($La_N/Sm_N = 2.22–8.30$). By contrast, two samples (YA1 and KPT5) display almost flat REE patterns ($La_N/Sm_N = 1.29–2.13$; $Sm_N/Dy_N = 0.71–0.99$).

Primitive-mantle (PM) normalised extended trace element patterns are shown in Fig. 6b. As for the REE, trace element compositions reflect the extreme depletion of these lithotypes, with concentrations ranging between 0.001 and 0.1 times PM values. Small positive anomalies can be detected for the fluid mobile elements (FME, i.e. Cs, Ba, Sr). Pb is strongly enriched (up to a factor of 1000) compared to the neighbouring Ce and Pr.

Overall, trace element composition of the New Caledonia harzburgites overlap those of the depleted harzburgites from the Izu-Bonin-Mariana region (Parkinson and Pearce, 1998), but they invariably display lower absolute concentrations for FME (i.e. Cs, Rb), HFSE (excepted KPT3, KPT5, PO3, YA1) and HREE (again with the exception of YA1 and KPT5 harzburgites).

Measured trace element concentrations are in the range of those provided by previous geochemical studies on the New Caledonia harzburgites (Marchesi et al., 2009; Ulrich et al., 2010).

4.3. Mineral trace element composition

Representative trace element compositions for orthopyroxene are reported in Table 2 and Supplementary Fig. S1.

Orthopyroxene compositions are homogeneous and reflect the extreme depletion of the whole rock, with REE contents mostly ranging between 0.001 and 0.1 times chondritic values. REE patterns are characterised by steep HREE ($Dy_N/Yb_N = 0.02–0.15$) and commonly exhibit enriched La–Ce segments. MREE are often below the detection limit. Neoblastic orthopyroxenes do not show any distinctive feature, having remarkably similar REE compositions compared to porphyroclastic orthopyroxenes. This could be related to subsolidus re-equilibration between porphyroclastic and

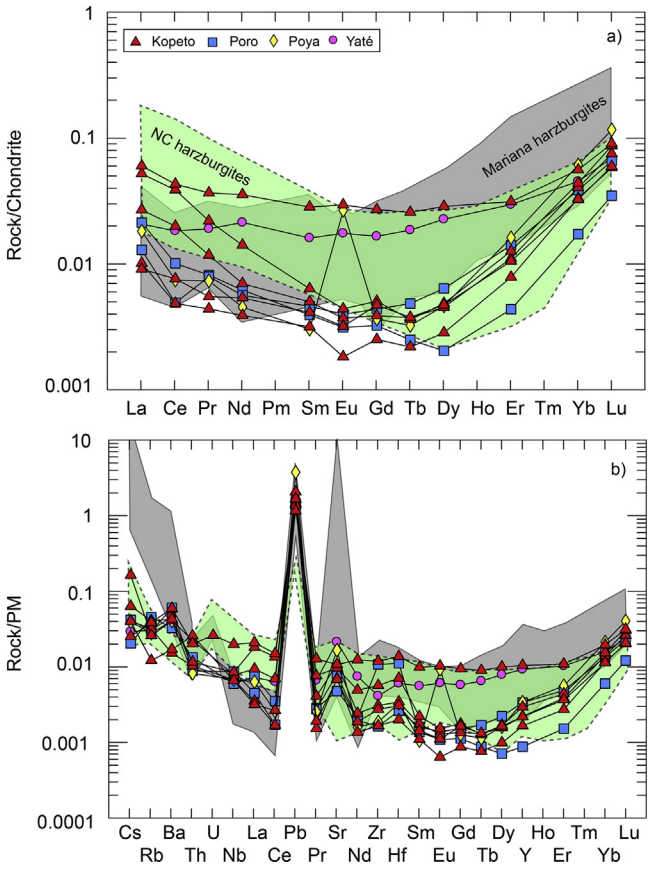

Fig. 6. (a) Whole-rock chondrite-normalised REE patterns for the New Caledonia harzburgites; normalising values are after Sun and McDonough (1989); (b) primitive mantle-normalised trace element patterns of the New Caledonia harzburgites. Normalising values are from Sun and McDonough (1989). In both diagrams, the grey area encloses the composition of Mariana harzburgites (Parkinson and Pearce, 1998), while light green area encompasses the composition of the New Caledonia harzburgites reported in the previous works of Marchesi et al. (2009) and Ulrich et al. (2010).

neoblastic orthopyroxene, i.e. to REE redistribution during cooling (Sun and Liang, 2014).

Olivine trace element contents are listed in Supplementary Table S2 and illustrated in Supplementary Fig. S2. REE concentrations of olivine are notably low, with most of the L- and some M-REE below the detection limit. HREE and MREE contents are always below 0.1 times chondritic values. HREE exhibit steeply to moderately sloping patterns (Dy_N/Yb_N = 0.08–1.25). Ti contents are also extremely low (0.12–0.65 ppm), in agreement with the ultra-depleted nature of these rock-types. Relatively high Pb concentrations (0.014–0.07 ppm) are recorded by olivine, mirroring whole rock Pb enrichments.

4.4. Geothermometry

Equilibrium temperatures for the harzburgites have been computed on the basis of mineral composition data obtained by microprobe and LA-ICP-MS analyses.

Due to the lack of primary clinopyroxene, Ca-in-orthopyroxene (Brey and Kohler, 1990; i.e. *T*(BK)), Ca-in-olivine (De Hoog et al., 2010; i.e. *T*(Ca in Ol)) and olivine-spinel geothermometers (i.e. *T*(Ol-Sp)) were applied to estimate the equilibrium temperatures of both porphyroclastic and neoblastic assemblages for an assumed confining pressure of 1.5 GPa.

The cores of orthopyroxene porphyroclasts yield *T*(BK) ranging between 950 and 1150 °C, displaying higher values compared to the estimates previously obtained by Pirard et al. (2013) using the same method (953–970 °C). Core-to rim compositional variations for orthopyroxene porphyroclasts locally reflect cooling of ca. 50–100 °C.

Temperatures provided by Ca-in-olivine and olivine-spinel geothermometers for the porphyroclastic assemblages testify significant cooling (*T*(Ca in Ol) = 800–850 °C; *T*(Ol-Sp) = 840–965 °C).

For the neoblastic orthopyroxene and olivine, calculated equilibrium temperatures are slightly lower (*T*(Ca in Ol) = 730–790 °C; *T*(BK) = 940–1065 °C). Remarkably lower temperatures have been also computed for the secondary orthopyroxene films (*T* = 810–850 °C).

Temperatures estimated using Ca–Mg exchange between secondary clino- and orthopyroxene vary between 916–932 °C and 924–966 °C, with a good agreement between Brey and Kohler (1990) and Taylor (1998) methods. In addition, single clinopyroxene thermometer of Nimis and Taylor (2000) provide values between 800 and 940 °C.

For the studied lithotypes pressure is difficult to constrain, owing the lack of appropriate geobarometers in garnet-free systems. The pressure of the garnet–spinel transition in peridotitic systems is mainly controlled by Cr content of the spinel (Webb and Wood, 1986; Klemme, 2004). In particular, spinel is stabilised to higher pressures with increasing Cr/(Cr + Al). A maximum pressure estimate for the spinel facies can be determined by using the formulation of Webb and Wood (1986). Using the composition of spinel porphyroclast cores the obtained pressures vary between 2.2 and 2.7 GPa.

4.5. Sr, Nd, Pb isotopes

Whole rock Sr, Nd and Pb isotope compositions are reported in Table 3 and illustrated in Figs. 7 and 8.

Initial $^{143}Nd/^{144}Nd$ of the harzburgites covers a wide range of values, extending from extremely depleted (PO4: $(^{143}Nd/^{144}Nd)_i$ = 0.51325, ε_{Nd_i} = +13.32) towards enriched compositions (KPT1-KPT5-PY1: $(^{143}Nd/^{144}Nd)_i$ = 0.51253–0.51278, $-0.80 \leq \varepsilon_{Nd_i} \leq +4.01$). Two samples (YA1, KPT3) display Nd isotopic signatures similar to a DMM source (Hofmann, 2003).

Sr isotopes mirror the same variability shown by Nd isotopes, varying between 0.70257 and 0.70770.

Initial $^{206}Pb/^{204}Pb$, $^{207}Pb/^{204}Pb$ and $^{208}Pb/^{204}Pb$ span between 18.038–18.638, 15.455–15.642 and 37.920–38.731, respectively. In the $^{208}Pb/^{204}Pb$ vs. $^{206}Pb/^{204}Pb$ vs. diagram (Fig. 8a), the harzburgites overlay the domain of the Indian-type MORB and define a broad positive trend, with three samples falling inside the field of the Pacific sediments (KPT1, PO4, PY1). By contrast, the other samples (KPT3, KPT5, YA1) show intermediate composition between the DMM and EM2/GLOSS pole.

In the $^{206}Pb/^{204}Pb$ vs. $^{207}Pb/^{204}Pb$ diagram (Fig. 8b), samples are more scattered and generally display high $^{207}Pb/^{204}Pb$, with some samples overlapping the field of the Pacific sediments (KPT1, PO4).

5. Discussion

5.1. Modelling mantle melting

Petrological indicators for the depletion degree in mantle peridotites (i.e. clinopyroxene modal abundance, Cr# of spinel, fusible and trace element concentrations) indicate that the New Caledonia harzburgites are highly refractory lithotypes, sharing remarkable similarities with modern subduction zone peridotites. The ultra-depleted nature of these lithotypes has been ascribed to a history of multiphase melting and involvement in the Eocene subduction system (Marchesi et al., 2009; Ulrich et al., 2010; Pirard et al., 2013).

Table 2
Orthopyroxene trace element composition (ppm) of the New Caledonia harzburgites. Trace element concentrations were determined by LA-ICP-MS.

Sample	KPT1	KPT1	KPT1	KPT3	KPT3	KPT3	KPT3	KPT3	KPT3	KPT5	KPT5	KPT5	KPT5	YA1	YA1	YA1
Pyrox name	KPT1_Opx6c	KPT1_Opx4	KPT1_Opx9	KPT3A_Opx2	KPT3A_Opx3c	KPT3A_Opx3r	KPT3A_Opx4c	KPT3A_Opx8c	KPT3A_Opx8r	KPT5_Opx3c	KPT5_Opx3r	KPT5_Opx6c	KPT5_Opx6c	YA1_Opx1r	YA1_Opx1r	YA1_Opx1c
Location	Kopeto	Kopeto	Kopeto	Kopeto	Kopeto	Kopeto	Kopeto	Kopeto	Kopeto	Kopeto	Kopeto	Kopeto	Kopeto	Yaté	Yaté	Yaté
Rock-type	Harz	Harz	Harz	Harz	Harz	Harz	Harz	Harz	Harz	Sp harz	Sp harz	Sp harz	Sp harz	Sp harz	Sp harz	Sp harz
Type	core	core	core	core	core	rim	core	core	rim	core	rim	core	core	rim	rim	core
Sc	20.78	20.15	22.54	22.89	25.15	22.45	25.62	23.67	21.97	23.75	23.47	23.51	23.16	22.36	22.57	22.88
Ti	6.7	6.6	7.0	6.4	6.2	5.7	6.1	5.4	5.2	4.2	4.2	4.4	4.5	1.1	1.2	1.1
V	61	57	61	83	86	82	85	88	83	61	61	65	66	47	50	50
Cr	5157	4257	4166	5214	5698	4454	5931	5920	5465	5313	5134	5758	5741	2927	3273	3488
Mn	957	957	967	968	970	1018	1001	1020	1037	1027	1025	998	1003	978	985	995
Co	52.6	51.2	49.6	55.8	53.5	54.5	55.4	56.1	57.3	52.7	52.6	55.2	54.8	49.2	50.3	54.6
Ni	668	629	612	703	686	669	734	688	738	653	645	713	707	599	613	664
Zn	32.5	31.5	29.2	32.9	31.7	32.6	32.9	32.4	34.2	33.0	32.6	32.8	32.8	29.4	30.7	32.1
Rb	bdl	bdl	bdl	0.39	bdl	bdl	bdl	bdl	bdl	bdl	bdl	bdl	bdl	bdl	0.01	0.02
Sr	bdl	bdl	0.01	bdl	bdl	bdl	bdl	bdl	0.01	bdl	bdl	bdl	bdl	0.04	0.10	0.28
Y	0.02	0.02	0.02	0.03	0.03	0.02	0.03	0.02	0.02	0.02	0.02	0.02	0.02	0.03	0.04	0.05
Zr	0.01	0.01	0.01	0.02	0.01	0.01	0.02	0.01	0.02	0.01	0.01	0.01	0.01	bdl	0.01	0.02
Nb	0.017	0.014	0.013	0.018	0.019	0.011	0.017	0.018	0.016	0.010	0.011	0.014	0.012	0.011	0.012	0.013
Cs	bdl	bdl	bdl	bdl	bdl	bdl	bdl	bdl	bdl	bdl	bdl	bdl	bdl	bdl	0.001	0.003
Ba	bdl	bdl	bdl	0.002	0.003	0.004	bdl	bdl	0.001	bdl	0.002	bdl	0.003	0.005	0.003	0.015
La	bdl	bdl	bdl	0.001	0.001	bdl	bdl	bdl	0.001	bdl	bdl	bdl	bdl	0.001	0.002	0.006
Ce	bdl	bdl	bdl	0.001	bdl	bdl	bdl	bdl	bdl	bdl	0.001	bdl	bdl	0.001	0.002	0.013
Pr	bdl	bdl	bdl	bdl	bdl	bdl	bdl	0.001	bdl	bdl	bdl	bdl	bdl	bdl	bdl	0.001
Nd	bdl	bdl	bdl	0.001	0.002	bdl	0.001	bdl	bdl	bdl	bdl	bdl	0.003	0.001	0.001	0.005
Sm	bdl	bdl	bdl	0.002	bdl	bdl	bdl	bdl	0.001	bdl	0.001	bdl	0.003	0.001	bdl	0.001
Eu	bdl	bdl	bdl	0.001	bdl	bdl	bdl	0.001	bdl	bdl	bdl	bdl	bdl	bdl	bdl	bdl
Gd	0.001	bdl	bdl	0.004	0.001	bdl	bdl	bdl	0.002	0.006	0.004	bdl	bdl	bdl	0.001	0.001
Tb	bdl	bdl	bdl	bdl	bdl	bdl	bdl	bdl	bdl	bdl	bdl	bdl	0.001	bdl	bdl	bdl
Dy	0.001	bdl	bdl	0.001	0.002	0.001	0.001	bdl	bdl	bdl	0.002	0.002	0.002	0.002	0.003	0.004
Ho	bdl	bdl	bdl	0.001	0.001	bdl	0.001	0.001	0.001	0.001	0.001	bdl	0.001	0.001	0.001	0.002
Er	0.007	0.004	0.007	0.008	0.008	0.004	0.007	0.005	0.003	0.005	0.006	0.008	0.005	0.005	0.006	0.009
Tm	0.002	0.002	0.002	0.002	0.002	0.002	0.002	0.002	0.002	0.001	0.002	0.002	0.002	0.001	0.001	0.002
Yb	0.024	0.025	0.031	0.026	0.028	0.028	0.030	0.030	0.017	0.023	0.020	0.028	0.026	0.018	0.017	0.020
Lu	0.005	0.005	0.005	0.008	0.007	0.007	0.008	0.007	0.007	0.006	0.007	0.007	0.006	0.004	0.005	0.005
Hf	bdl	bdl	bdl	0.001	0.003	0.001	0.001	0.002	bdl	bdl	bdl	bdl	0.001	0.001	bdl	bdl
Pb	0.054	0.051	0.049	0.043	0.044	0.036	0.021	0.017	0.037	0.020	0.065	0.075	0.018	0.173	0.112	0.100
Th	bdl	bdl	bdl	bdl	bdl	bdl	bdl	bdl	bdl	bdl	bdl	0.001	bdl	0.001	0.003	0.003
U	bdl	bdl	bdl	bdl	bdl	bdl	bdl	bdl	bdl	bdl	bdl	bdl	bdl	bdl	0.002	0.001
Dy_N/Yb_N	0.020	-	-	0.027	0.025	0.030	0.048	-	-	-	0.054	0.037	0.063	0.058	0.106	0.149
Yb_N	0.142	0.146	0.184	0.153	0.166	0.162	0.175	0.174	0.098	0.134	0.118	0.162	0.151	0.107	0.099	0.119

Note: bdl, below detection limit.

Table 3
Whole rock Sr, Nd and Pb isotopic compositions of the New Caledonia harzburgites. Uncertainities (±2σ) refer to within-run precision, given as standard error on the mean (SE) quoted at the 95% confidence level. ε_{Sr} and ε_{Nd} values were calculated as deviation from a chondritic uniform reservoir (CHUR) with present-day $^{86}Sr/^{87}Sr = 0.70448$,$^{87}Rb/^{85}Rb = 0.0816$,$^{143}Nd/^{144}Nd = 0.512638$,$^{147}Sm/^{144}Nd = 0.1966$.

Sample	KPT1	KPT3	KPT5	KPT5 dupl	PO4	PY1	YA1	YA1 dupl
Type	*WR*	*WR*	*WR*	*WR*	*WR*	*WR*	*WR*	*WR*
Location	Kopeto	Kopeto	Kopeto	Kopeto	Poro	Poya	Yaté	Yaté
Measured ratio								
$^{143}Nd/^{144}Nd$	0.51259 ± 9	0.51310 ± 16	0.51282 ± 1	0.51287 ± 2	0.51331 ± 8	0.51282 ± 7	0.51310 ± 1	0.51304 ± 2
Sm (ppm)	0.0005	0.0010	0.0043	0.0043	0.0007	0.0005	0.0024	0.0024
Nd (ppm)	0.0018	0.0065	0.0166	0.0166	0.0026	0.0021	0.0099	0.0099
$^{147}Sm/^{144}Nd$	0.160		0.158	0.158	0.162	0.132	0.148	0.148
$^{87}Sr/^{86}Sr$	0.707998 ± 46	0.707868 ± 18	0.706725 ± 7		0.705646 ± 25	0.706957 ± 32	0.702667 ± 8	
Rb (ppm)	0.020	0.026	0.025		0.019	0.018	0.019	
Sr (ppm)	0.145	0.200	0.224		0.167	0.348	0.447	
$^{87}Rb/^{86}Sr$	0.398	0.374	0.317		0.323	0.147	0.125	
$^{208}Pb/^{204}Pb$	38.7316 ± 13	37.9196 ± 6	38.0102 ± 10		38.6794 ± 15	38.6157 ± 54	38.0609 ± 21	
$^{207}Pb/^{204}Pb$	15.6395 ± 5	15.5980 ± 2	15.4553 ± 10		15.6418 ± 5	15.5606 ± 21	15.5943 ± 8	
$^{206}Pb/^{204}Pb$	18.6386 ± 10	18.0381 ± 2	18.2268 ± 20		18.6127 ± 6	18.5717 ± 24	18.1885 ± 9	
Age corrected ratio (53 Ma)								
$(^{143}Nd/^{144}Nd)_i$	0.51253	0.51307	0.51276	0.51282	0.51325	0.51278	0.51305	0.51299
ε_{Nd_i}	−0.80	+9.76	+3.69	+4.81	+13.32	+4.01	+9.28	+8.18
$(^{87}Sr/^{86}Sr)_i$	0.707698	0.707586	0.706487	0.706487	0.705402534	0.706846	0.702573	0.702573
ε_{Sr_i}	46.26	44.69	29.07	29.07	13.68422379	34.18	−26.48	−26.48
$^{208}Pb/^{204}Pb$	38.7310	37.9196	38.0102		38.6789	38.6157	38.0604	
$^{207}Pb/^{204}Pb$	15.6395	15.5980	15.4553		15.6418	15.5606	15.5942	
$^{206}Pb/^{204}Pb$	18.6380	18.0381	18.2268		18.6119	18.5717	18.1879	

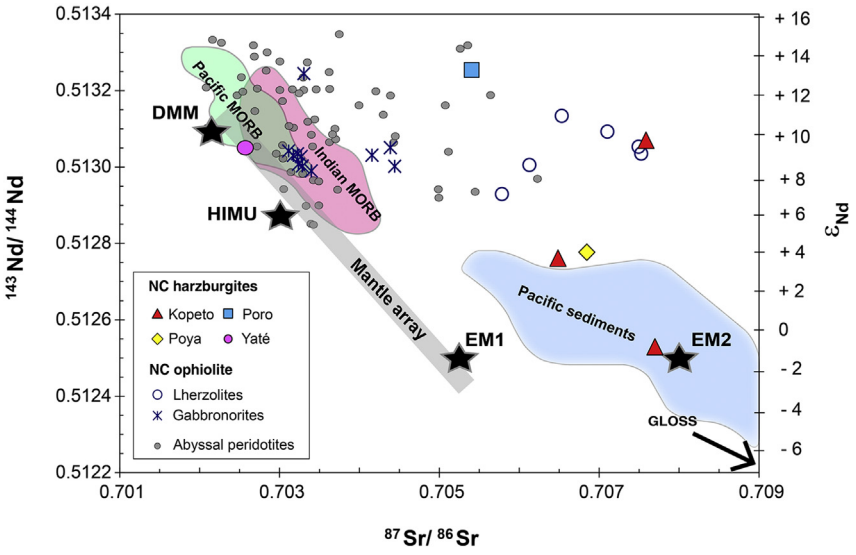

Fig. 7. Age-corrected (53 Ma), $^{87}Sr/^{86}Sr$ vs. $^{143}Nd/^{144}Nd$ diagram for the New Caledonia harzburgites. The pink and pale green fields include Indian and Pacific-type MORB data, respectively (Hofmann, 2003). Grey dots: abyssal peridotites from Central and Southern Atlantic (Snow and Dick, 1995; Cipriani et al., 2004) and South West Indian ridge (Salters and Dick, 2002; Warren et al., 2009). Sr and Nd isotopic composition of the New Caledonia lherzolites and gabbronorites are from Secchiari et al. (2016) and Secchiari et al. (2018), respectively. Sediments field encloses data from Othman et al. (1989), PetDB and GERM database (http://www.earthchem.org/petdb; https://earthref.org/GERM/). Main mantle reservoir data after Zindler and Hart (1986) and Eisele et al. (2002).

In order to evaluate if bulk rock major element variations in the harzburgites are the result of partial melting, the compositional trends of the harzburgites have been compared in Fig. 5 with the anhydrous melting curves calculated by Herzberg (2004). As a whole, the harzburgites have exceedingly low Al_2O_3, compatible with very high degrees of melting (up to 25%–30%) at $P \leq 2$ GPa, whereas in the SiO_2-MgO diagram all the samples plot off the melting curves of Herzberg (2004), most likely due to the crystallisation of secondary orthopyroxene leading to SiO_2 enrichment.

The observed major element trends hint that the widespread occurrence of orthopyroxene embayments filled by olivine in the harzburgites may be ascribed to incongruent melting of orthopyroxene, characteristic of decompression melting beneath oceanic ridges (Niu, 1997). These textures have been also interpreted as the result of reactive porous flow of pyroxene-undersaturated melts (e.g. Piccardo et al., 2007; Rampone et al., 2008). However, the absence of chemical evidence, such as the decrease of SiO_2 and increase of FeO^t against MgO, resulting from olivine addition during melt migration, rule out this interpretation.

A raw estimate of the degree of partial melting experienced by the harzburgites can be obtained following the method of Hellebrand et al. (2001), which is based on the Cr# value of spinel

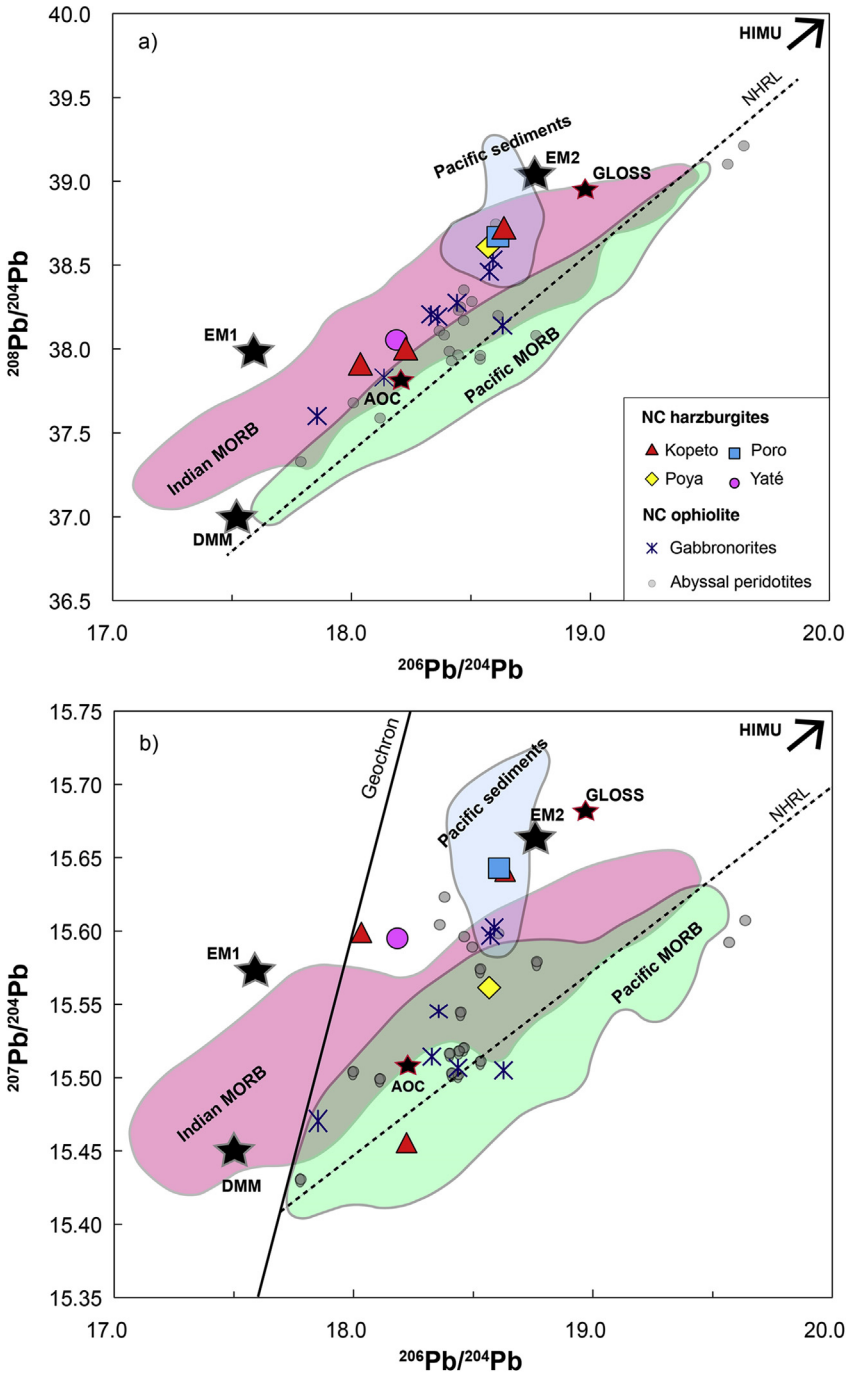

Fig. 8. Age-corrected (i.e. 53 Ma) $^{206}Pb/^{204}Pb$ vs. (a) $^{208}Pb/^{204}Pb$ and (b) $^{207}Pb/^{204}Pb$ diagram for the New Caledonia harzburgites. New Caledonia lherzolites and gabbronorites data after Secchiari et al. (2016) and Secchiari et al. (2018). Pink and pale green fields: Indian and Pacific MORB, respectively (Hofmann, 2003). Pacific sediments field includes data from Othman et al. (1989), Elliott et al. (1997), Hemming and McLennan (2001), Plank (2013), PetDB and GERM database (http://www.earthchem.org/petdb; https://earthref.org/GERM/). GLOSS composition is after Plank and Langmuir (1998). Black, dotted line = Northern Hemisphere Reference Line (NHRL).

($F = 10 \times (\ln Cr\#) + 24$). Applying this equation to the spinel porphyroclast cores of the harzburgites (Supplementary Table S1), partial melting degrees ranging between 17% and 20% were computed. This method, however, may underestimate the degree of bulk melting of the peridotites, as Cr# values can be strongly affected by subsequent refertilisation.

In order to constrain more accurately the melting process that produced the trace element variations observed for the New Caledonia harzburgites, geochemical modelling based on whole rock and orthopyroxene compositions has been carried out. We compared two non-modal fractional melting models, both occurring entirely in the spinel stability field.

In the first scenario, we applied a non-modal fractional melting model using the equations of Shaw (1970), assuming a single-stage melting of a DM source (Salters and Stracke, 2004). Details about the model and partition coefficients (Ionov et al., 2002) are given in Supplementary Table S3. Percentages of partial melting were calculated on the basis of the HREE contents, as LREE and MREE in peridotites are easily affected by metasomatism (e.g. Vernières et al., 1997; Niu, 2004). Results show that the HREE compositions

of the harzburgites require very high degrees of partial melting, between 20% and 25% (Supplementary Fig. S3), in agreement with the previous estimates obtained by Marchesi et al. (2009) and Ulrich et al. (2010). By contrast, LREE and MREE appear much more enriched compared to the values expected for the corresponding melting degrees. Such high melting degrees are unlikely to occur in mid-ocean ridge environment, while they are commonly recorded in subduction zone setting (e.g. Parkinson and Pearce, 1998; Bizimis et al., 2000; Zanetti et al., 2006), where slab-derived fluids enhance melting by lowering peridotite solidus (Mysen and Boettcher, 1975; Stolper and Newman, 1994; Hirschmann et al., 1999).

Secondly, a two-stage melting model, including dry melting of a DM source (Salters and Stracke, 2004) and re-melting under hydrous conditions, has been performed. This model was based on both whole rock and orthopyroxene trace element compositions. A summary of melting parameters is provided in Supplementary Table S3. In this model, trace element concentrations (Nb, La, Ce, Sr, Nd, Zr, Hf, Sm, Eu, Ti, Y, Er, Yb, Lu) were calculated for a solid peridotitic residue left after 15% degrees of non-modal fractional melting. The residue was then used as starting composition for the second melting phase. The second melting stage has been modelled as fractional, non-modal hydrous melting until clinopyroxene consumption (for F = 13%, where F represents the melting degree).

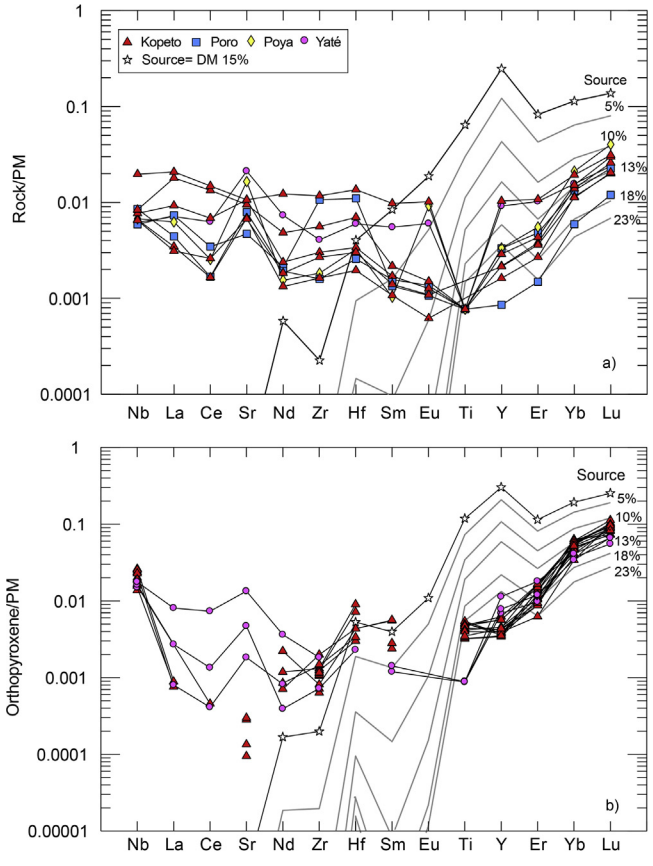

Fig. 9. PM-normalised trace element patterns compared to melting curves (light grey) for: (a) whole rock and (b) orthopyroxene in equilibrium with whole rock. Melting curves have been calculated in different steps using a peridotitic residue left after 15% non-modal fractional melting (dry melting) of a DM source (Salters and Stracke, 2004) in the spinel stability field as a starting material. Numbers close to melting curves: melting degrees referred to the starting mantle source. Melting curves represent non-modal, hydrous, fractional melting in the spinel stability field until clinopyroxene exhaustion (F = 13%). After clinopyroxene consumption, melting curves have been computed through modal batch melting, following the approach of König et al. (2010). See text for further details. Melting modes and crystal/liquid partition coefficients are reported in Supplementary Table S3.

We refer to hydrous melting to describe a mantle source that melts following a hydrous melting reaction (Gaetani and Grove, 1998), but no fluid-mobile elements were added during melting. We used partition coefficients between minerals and melt that were experimentally constrained during hydrous melting at shallow upper mantle conditions (McDade et al., 2003). Modal abundances were recalculated at each step (1% melting at each step) and element concentrations in the source were taken from the composition of the residue in equilibrium with the melt from the step before. After clinopyroxene exhaustion, a modal batch melting model under hydrous conditions was applied, following the approach developed by König et al. (2010).

Results for melting models are presented in Fig. 9a and b. In order to reach the highly depleted HREE contents observed for the harzburgites, 10%–18% melting degrees of a mantle residue left after 15% degrees of partial dry melting are necessary. The obtained results show that the HREE patterns of the New Caledonia harzburgites can be reproduced by melting in the spinel field alone without invoking deeper melting under garnet-facies conditions. In fact, the presence of symplectitic spinel-pyroxene aggregates have been recently related both tolate stage melt-rock reactions or to the cooling evolution of the harzburgites (see Secchiari et al., 2019).

Although the calculated patterns reasonably fit the observed whole rock and orthopyroxene HREE compositions, Y and Ti invariably display more depleted compositions than expected, while Sr, Nb, Zr, Hf, LREE and MREE are enriched, requiring syn- and/or post-melting metasomatic processes (see sections 5.2 and 5.3). Similar depletion features for Ti, associated with LREE-MREE enrichment, have been also observed in the refractory mantle xenoliths from Papua New Guinea, where they have been ascribed to Ti loss during late stage metasomatism (Grégoire et al., 2001).

Despite both melting models illustrated above may reproduce HREE contents of the harzburgites, they reflect different physical processes. A single stage model would imply very high degrees of melting beneath the supra-subduction zone (yielding large volume of melt fractions), induced by large H_2O fluxes from the downgoing slab. Conversely, in the two-stage model, prior melting would occur in a mid ocean ridge setting (dry melting), and the mantle would subsequently undergo fluid-assisted melting beneath the supra-subduction zone, with lower H_2O input to the source.

For the New Caledonia harzburgites, FME enrichments are recorded by both whole rock and orthopyroxene. However, the absolute concentrations of these elements are too low to be reconciled with the large fluid fluxes assumed by the first model (see also discussion in the paragraphs 5.2 and 5.3). In addition, the first melting scenario is not consistent with the tectonic evolution of the New Caledonia archipelago. The period from the Campanian to Paleocene is in fact marked by the opening of marginal basins followed by intra-oceanic subduction during Eocene. Recently, Ulrich et al. (2010) have proposed that the subduction started close to or in correspondence of an active oceanic spreading center, where relatively hot and young (~6–9 Myr old; Cluzel et al., 2016) lithosphere was forced to subduct. Large fluid fluxes thus appear unlikely, owing to the young age of the subducted material and the intra-oceanic nature of the subduction, which probably prevented the presence of large volumes of sediments (Cluzel et al., 2016). We therefore conclude that the second melting model (i.e. dry melting followed by hydrous melting) depicts a more plausibile scenario given the geodynamic evolution of the south western Pacific mantle.

5.2. Constraints on fluid-mobile element enrichment of the mantle wedge peridotite during hydrous melting

In the previous paragraph we have shown that several geochemical features displayed by the harzburgites, namely FME

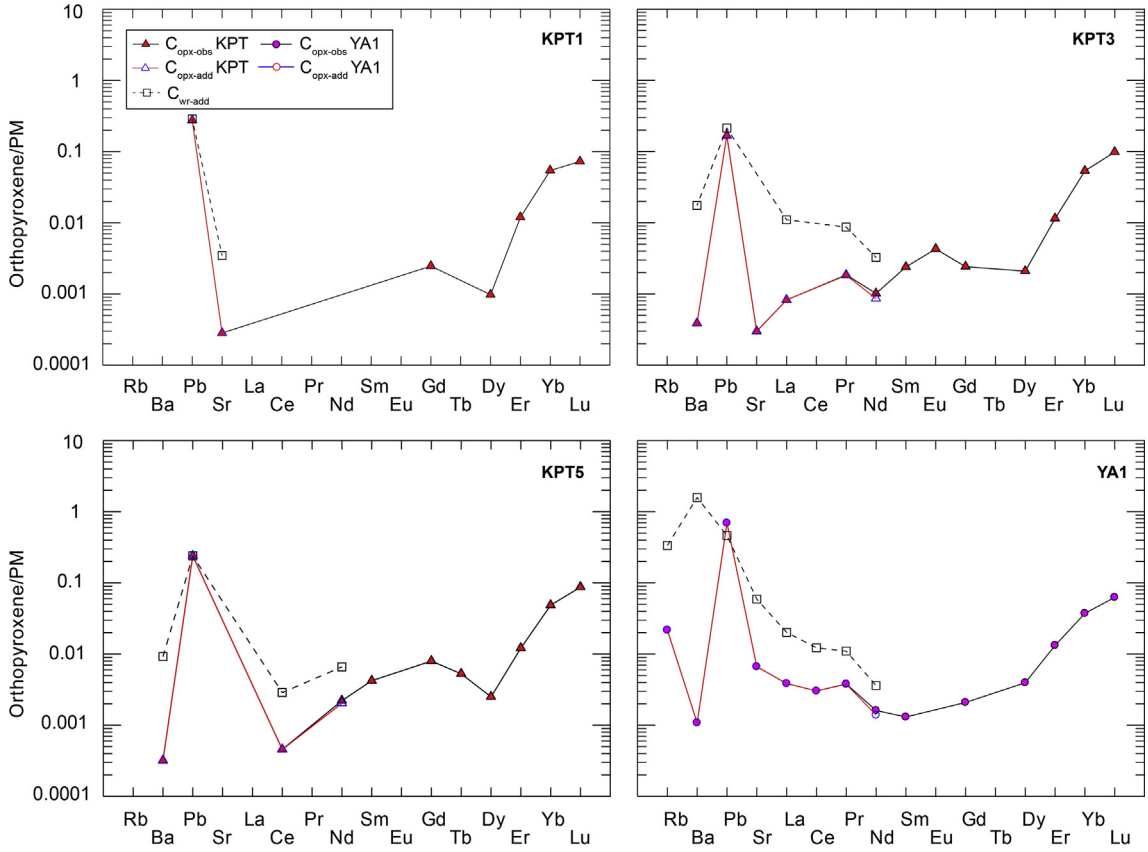

Fig. 10. PM-normalised compositions of the fluid-added to orthopyroxene ($C_{opx\text{-}add}$) and to whole rock ($C_{wr\text{-}add}$) compared to the average observed compositions ($C_{opx\text{-}obs}$). Values have been calculated using the algorithm of Shervais and Jean (2012). Normalising values after Sun and McDonough (1989).

Table 4
Results from fluid addition calculation at 0.1% melt increment of a DM source (Salters and Stracke, 2004) left after 15% degrees of melting. $C_{opx\text{-}obs}$ = concentration of observed orthopyroxene; $C_{wr\text{-}added}$ or $C_{opx\text{-}added}$ = concentration of FME added to whole rock or orthopyroxene during a given melt increment.

Sample	KPT1			KPT3			KPT5			YA1		
	$C_{opx\text{-}obs}$	$C_{wr\text{-}added}$	$C_{opx\text{-}added}$	$C_{opx\text{-}obs}$	$C_{wr\text{-}added}$	$C_{opx\text{-}added}$	$C_{opx\text{-}obs}$	$C_{wr\text{-}added}$	$C_{opx\text{-}added}$	$C_{opx\text{-}obs}$	$C_{wr\text{-}added}$	$C_{opx\text{-}added}$
Rb	bdl	-	-	bdl	-	-	bdl	-	-	0.0138	0.2129	0.0138
Ba	bdl	-	-	0.0027	0.1221	0.0027	0.0022	0.0644	0.0022	0.0076	11.0682	0.0076
Pb	0.0509	0.0532	0.0509	0.0309	0.0394	0.0309	0.0443	0.0443	0.0443	0.1283	0.0855	0.1283
Sr	0.0060	0.0731	0.0059	0.0063	0.0904	0.0063	bdl	-	-	0.1402	1.2448	0.1402
La	bdl	-	-	0.0006	0.0076	0.0006	bdl	-	-	0.0027	0.0138	0.0026
Ce	bdl	-	-	bdl	-	-	0.0008	0.0051	0.0008	0.0054	0.0218	0.0054

contents, as well as Nb, Zr, Hf, LREE and MREE, cannot be ascribed to a simple history of melting depletion. At a first approximation we consider that interaction with slab-related hydrous fluids during melting may explain the FME enrichments.

In order to constrain FME fluxes in the mantle wedge, we have applied the algorithm presented by Shervais and Jean (2012) and modified by Jean and Shervais (2017) for four selected samples (KPT1, KPT3, KPT5, YA1). This algorithm allows to model the fluid enrichment process and determine the amount of subduction component added to the mantle wedge peridotite for each melt increment, starting from orthopyroxene trace element composition. Orthopyroxene trace element composition constitutes a powerful tool for assessing depletion and enrichment history of mantle peridotites, especially in mantle sections that have experienced complete consumption of clinopyroxene, offering important petrological insights into the evolution of refractory peridotites (e.g. Scott et al., 2016).

Details of the parameters used in the algorithm and results are provided in Fig. 10, Table 4 and Supplementary Table S4. To apply the calculator, we have first adjusted the melt fractions (F) together with the retained melt fraction input, in order to obtain a close fit between the MREE-HREE of the model with the observed orthopyroxene. When the solutions for any element exceed the model abundances, i.e. values expected from melting without any addition of slab material, the excess needs to be interpreted in terms of addition of subduction material to the mantle wedge peridotite. Fluid-mobile elements (Rb, Ba, Pb, Sr) are enriched compared to their model abundances both in orthopyroxene and whole-rock. $C_{opx,add}$ were 0.014 ppm for Rb, 0.002–0.008 ppm for Ba, 0.03–0.14 ppm for Pb and 0.06–0.14 ppm for Sr. Larger amounts were calculated for whole rock addition (Rb = 0.21 ppm, Ba = 0.06–11.1 ppm, Pb = 0.04–0.08 ppm, Sr = 0.07–1.24 ppm). Similar values are consistent with the previous estimates of FME

fluxes for the Coast Range ophiolite rock-types obtained by Shervais and Jean (2012) and Jean and Shervais (2017).

Another important observation lies in the fact that LREE may be explained by fluid addition to the mantle wedge, while the small enrichments of Th, Zr and MREE (not reported) fail to be reproduced in this way. To explain such contrasting behaviour, post-melting interaction with slab-derived melts or hydrous fluids containing small fractions of dissolved silicate melt may be required.

5.3. Post-melting enrichment processes

High degrees of melt extraction can account for some major and trace element variations observed in the harzburgites, but the enrichments of several incompatible trace elements (namely FME, LREE and MREE, Nb, Zr, Hf) recorded by whole rocks and orthopyroxene (Figs. 6a, b and 9a, b), are not consistent with the highly residual character testified by HREE. In the previous section we have illustrated how FME enrichments may be accounted by slab input during fluid-assisted melting, whereas different processes are probably needed to explain the abundances of the other incompatible trace elements.

First, melting with relatively high porosities (>5%) may have caused retention of unextracted fractions of melt, leading to crystallization of new interstitial phases and consequent increase of incompatible trace element concentrations. However, this would also cause a concomitant increase of HREE contents both in whole rock and orthopyroxene, which is in contrast with the observed compositions.

On the other hand, the occurrence of ortho- and clinopyroxenes interstitial with respect to the neoblastic pyroxene-olivine aggregates (Fig. 3e) suggest that the harzburgites may have undergone post-melting enrichment related to secondary phase formation. Secondary pyroxenes in the studied harzburgites have major element compositions similar to those found in arc xenoliths from southern Kamchatka (Avacha volcano, e.g. Ishimaru et al., 2007; Arai and Ishimaru, 2008), Philippines (Iraya volcano, e.g. Arai, 2004) and New Guinea (Lihir islands, e.g. McInnes et al., 2001). These phases have been ascribed to mantle wedge metasomatism operated by slab-derived aqueous fluids (containing a dissolved silicate component) or by hydrous silicate melts (e.g Arai et al., 2003, 2004; Ishimaru et al., 2007). Irrespective of their ultimate origin, such fluids are rich in SiO_2 relative to MgO (e.g. Mibe et al., 2002) and have the potential to convert olivine to orthopyroxene, thus promoting silica enrichment in the mantle wedge peridotites. Remarkably, formation of metasomatic orthopyroxene from primary olivine (Fig. 3h) and whole rock silica enrichment (Fig. 5) have been observed in the harzbugites of this study. The widespread occurrence of secondary pyroxenes may thus bear witness of interaction between the harzburgites and a subduction-related component. The nature of the metasomatic agent leading to secondary pyroxene crystallization (silicate-bearing aqueous fluid vs. melt) and its source are difficult to constrain. However, the enrichments of the residual peridotites in Nb, Zr, Hf and MREE (Fig. 9a, b) favour interaction with a silicate melt (e.g. see Parkinson and Pearce, 1998). Although trace element information are not available because their very small size prevented in situ trace element analysis, Nb, Zr, Hf and MREE may be mainly accommodated by clinopyroxene, as hydrous partition coefficients for clinopyroxene are one order of magnitude higher compared to orthopyroxene (Brenan et al., 1995; McDade et al., 2003).

Geochemical and petrological studies on mantle wedge peridotites and arc xenoliths have emphasised the importance of adakite-like melts as metasomatic agents above subduction zones (e.g. Ishimaru et al., 2007; Arai and Ishimaru, 2008; Grégoire et al., 2008). For the New Caledonia archipelago, young and buoyant oceanic crust is thought to have been involved in the subduction zone system at the beginning of the Eocene convergence (e.g. Ulrich et al., 2010; Cluzel et al., 2012b, 2016), making adakitic melts a plausible metasomatic agent. In addition, the presence of granitoid dykes crosscutting the ultramafic rocks has been testified in the New Caledonia ophiolite. These dykes are believed to reflect the

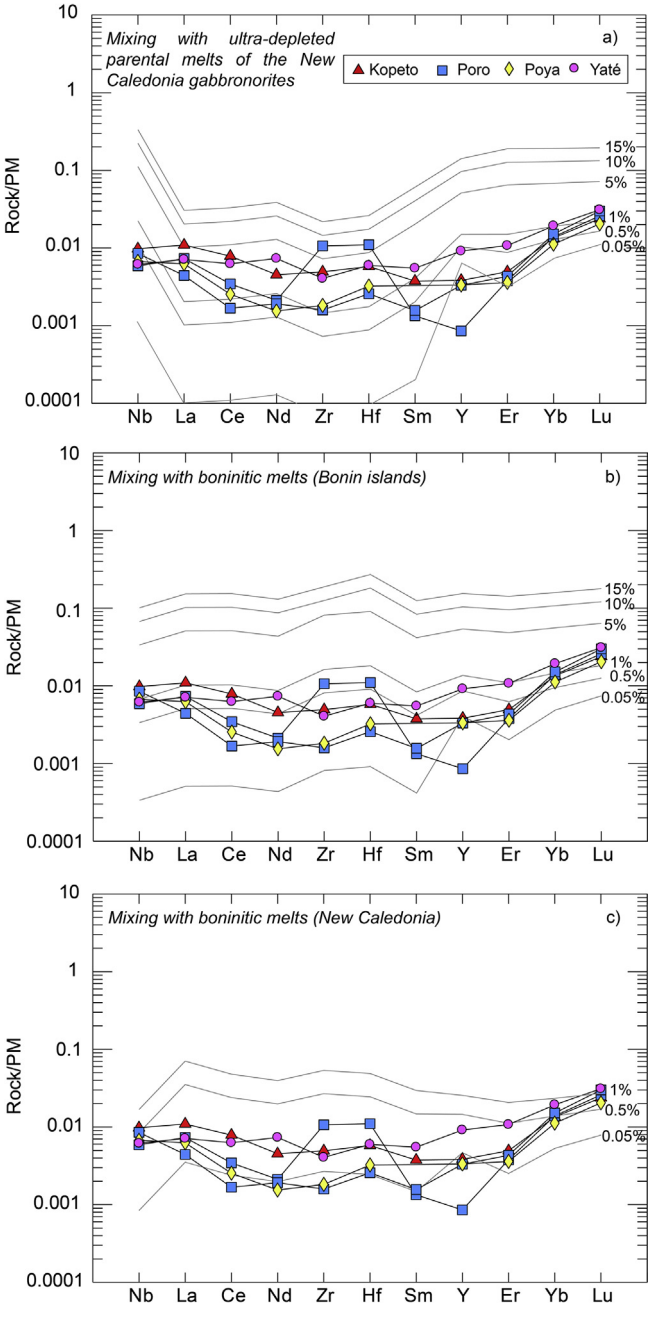

Fig. 11. Primitive mantle-normalised whole-rock abundances of REE-Nb-Zr-Hf-Y calculated for variable trapped melt modes (%) in a highly depleted harzburgite. The calculated whole rock compositions are compared with the New Caledonia harzburgites. The impregnating liquids were an ultra-depleted melt, whose composition has been obtained calculating average composition of: (a) parental melts of the New Caledonia gabbronorites (Secchiari et al., 2018); (b) and (c) boninitic melts from Bonin islands (Li et al., 2013) and New Caledonia (Cluzel et al., 2016), respectively. Further details are reported in Supplementary Table S5.

first subduction-triggered magmatic pulses originated from melting of garnet-bearing mafic protoliths (Cluzel et al., 2006). Nevertheless, interactions between a peridotite assemblage and different adakitic melts at 1.5 GPa are expected to form either orthopyroxene together with Na_2O-rich amphibole and phlogopite (Prouteau et al., 2001) or ortho- and clinopyroxene with significantly higher Al_2O_3 and Na_2O contents than those observed in the investigated samples (Coogan et al., 2002). Another possible explanation may involve interaction with small fractions of subduction-related melts with depleted incompatible trace element compositions, like those produced during the inception of magmatic activity in convergent settings (i.e. boninites or transitional types towards island arc tholeiites, see Stern et al., 2012). To test this hypothesis from a geochemical point of view, we have simulated the chemical effect of simple melt entrapment in a highly residual harzburgite for a set of incompatible trace elements (Nb, La, Ce, Nd, Zr, Hf, Sm, Y, Er, Yb, Lu). Detailed information about the composition of the starting material and the metasomatic agents are reported in Supplementary Table S5. We have assumed as initial protholith a mantle residue left after 15% degrees of dry melting followed by 18% degrees of hydrous melting, corresponding to the HREE compositions of the most depleted samples in our dataset. Mixing with boninitic melts (Li et al., 2013; Cluzel et al., 2016) and the ultra-depleted parental liquids inferred for the New Caledonia gabbronorites (Secchiari et al., 2018) have been considered. The resulting trace element concentrations are reported for illustrative purpose in Fig. 11. As a whole, these simple models show that entrapment of even negligible melt fractions has a striking influence on the incompatible trace element budget of highly depleted residues. A more realistic scenario may involve a reactive process where the infiltrating melts dissolve olivine crystallising ortho- and clinopyroxene, in agreement with textural and mineralogical evidences. We thus propose that the observed enrichments in terms of LREE, MREE and some HFSE mainly reflect post-melting interaction between the harzburgites and small-volume migrating melts. Afterwards, the formation of tremolitic amphibole, often in association with talc (Fig. 3b, g) may represent a late stage fluid infiltration at relatively high T (up to 650–700 °C; O'Hara and Ishii, 1998; see also Soret et al., 2016) which may have further contributed to modify the FME budget of the harzburgites.

5.4. Isotopic constraints on the mantle source

As shown in Fig. 7, the harzburgites display a wide range of Sr–Nd isotopic signatures, which are mirrored by Pb isotopic compositions (Fig. 8).

The isotopic signature shown by arc rocks is thought to reflect a "hybrid signature", inherited from interaction between the mantle wedge peridotite and fluid or melts coming from the altered oceanic crust and/or sediments of the subducting plate (e.g. Dhuime et al., 2007). Hence, different end-members need to be taken into account in order to explain the isotopic signature of the studied harzburgites.

Based on Nd isotopic ratios, three distinct isotopic signatures can be identified: (1) a depleted, MORB-type signature; (2) an ultra-depleted signature and (3) an enriched, "sediment-like" composition.

Two samples (YA1, KPT3) exhibit similar Nd isotopic ratios ($+9.28 \leq \varepsilon_{Nd_i} \leq +9.76$), in the range of a DMM source (Hofmann, 2003). These compositions fall in field of the abyssal-type peridotites and are remarkably similar to the values recorded for the New Caledonia lherzolites (Secchiari et al., 2016). As the New Caledonia lherzolites do not display geochemical features indicative of involvement in the subduction system, we can assume these compositions as representative of the mantle source unaffected by subduction components. However, KPT3 shows higher $(^{87}Sr/^{86}Sr)_i$(0.70759) compared to YA1 harzburgite (0.70257). The higher $(^{87}Sr/^{86}Sr)_i$ of KPT3 is unlikely to be linked to hydrothermal alteration, as the sample is very fresh with a low value of loss on ignition (see Table 1). Moreover, the harzburgite with the lowest $(^{87}Sr/^{86}Sr)_i$ is actually the more altered sample in out dataset (i.e. YA1, LOI = 6.83 wt.%). We thus exclude that the higher $(^{87}Sr/^{86}Sr)_i$ displayed by KPT3 could be related to seawater-related alteration. By contrast, the higher Sr isotopic ratio, coupled with enrichment in the most incompatible elements, could be reconciled with contamination by small amount of a subduction-related component.

Among the studied samples, harzburgite PO4 displays a very radiogenic Nd isotopic composition ($\varepsilon_{Nd_i} = +13.32$), plotting at the more radiogenic end of the depleted MORB mantle sources (Salters and Stracke, 2004; Workman and Hart, 2005). Such highly radiogenic isotopic ratio is indicative of a mantle reservoir that experienced long-term depletion of Nd. Extremely radiogenic Nd–Hf and poorly radiogenic Os–Pb isotopic signatures have been recorded in the modern oceanic mantle (e.g. Liu et al., 2008; Stracke et al., 2011; Warren and Shirey, 2012). These signatures have been ascribed to the presence of refractory mantle domains registering ancient depletion events (up to 2 Ga, e.g. Harvey et al., 2006; Liu et al., 2008).

Remarkably, we note that in the New Caledonia peridotite similar radiogenic isotopic signatures have also been reported for the mafic sequence overlying the harzburgite tectonites (e.g. Secchiari et al., 2018), suggesting melting of a refractory mantle source.

Three samples (KPT1, KPT5, PY1) in our dataset yield poorly radiogenic Nd isotopic ratios ($-0.80 \leq \varepsilon_{Nd_i} \leq +4.01$) coupled with high $(^{87}Sr/^{86}Sr)_i$ (0.70649–0.70770), plotting close to or in the field of Pacific sediments. Such enriched isotopic signatures are unlikely to occur in a MORB-type mantle and are consistent with interaction between the mantle source and a subduction component. In the previous sections we have shown that the New Caledonia harzburgite experienced syn- to post-melting evolution including contamination by slab-derived hydrous fluids associated with FME enrichment and percolation by melts with a depleted trace element signature (e.g. boninite-like), leading to precipitation of secondary metasomatic phases. In order to verify if the Sr–Nd isotopic systematics could have been influenced by these events, we have performed a simple mixing model to simulate interaction between

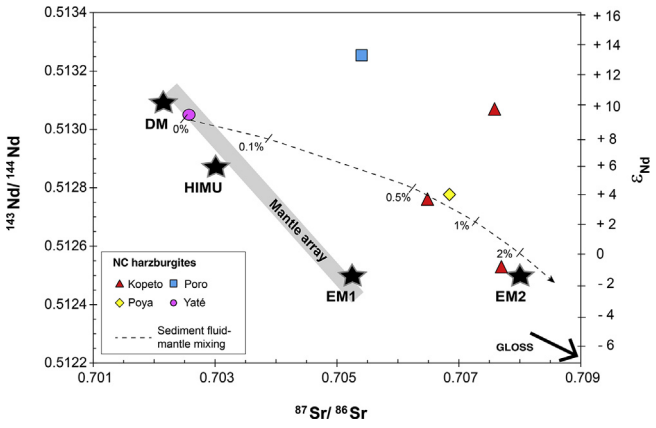

Fig. 12. Initial Sr and Nd isotopic diagram for the New Caledonia harzburgites. Black dashed arrow line represents mixing line between mantle wedge and fluids from sediment. For detailed explanation and end-members composition refer to text (section 5.4) and Supplementary Table S6.

the mantle source and a component derived from the subducting sediments. End-member compositions and model parameters are shown in Supplementary Table S6. The choice of end-member compositions is the most critical issue for a mixing model due to diversity of compositions of subducted sediments and oceanic crust, but also to the difficult choice of an appropriate mantle source composition. Due to the lack of direct information concerning the composition of the subducted material during the Eocene convergence, we assumed that isotopic compositions of the subducted sediments and oceanic crust were similar to those of the Pacific plate sediments and oceanic crust, which have been used for modelling geochemical characteristics of the Izu-Bonin arc (Ishizuka et al., 2003). To model the initial trace element and Sr–Nd composition of the New Caledonia mantle source before subduction, we have considered the average chemical and isotopic composition of lherzolites taken from Secchiari et al. (2016). Results of the model are reported in Fig. 12. Addition of 0.5%–2% of sediment-derived fluids to the mantle wedge reasonably accounts for the Sr–Nd isotopic compositions of the most enriched samples in our dataset (see Fig. 12).

Contamination of the harzburgites by a subduction-related component of sedimentary origin seems also consistent with their Pb isotopic signatures. In the $^{206}Pb/^{204}Pb$ vs. $^{208}Pb/^{204}Pb$ isotopic diagram (Fig. 8a), the samples define a linear trend extending from DMM toward enriched, sediment-like compositions. However, similar trends have been observed forarc rocks worldwide (Dhuime et al., 2007) and have been interpreted to reflect either (1) a mantle source represented as a single component in the context of mantle end-members (i.e. an Indian-type mantle reservoir) or (2) a mantle source that experienced contamination by a subduction component (e.g. fluids released from dehydration of sediments from the downgoing slab).

The involvement of Indian-type mantle in the Western Pacific arcs, from Izu-Bonin islands southward, has been proposed by several authors on the basis of the Nd–Hf–Pb isotopic signal of the Pacific lavas (e.g. Hickey-Vargas et al., 1995; Mahoney et al., 1998). The Indian-type mantle affinity displayed by some Pacific arc lavas has been ascribed to the presence of old sub-Gondwana lithosphere in the Pacific mantle wedges (e.g. Kamenov et al., 2008; Schuth et al., 2011). In particular, in the SW Pacific area, the occurrence of an Indian-type source has been attested in the Papuan archipelago (e.g. Schuth et al., 2004) and in the Vanuatu islands (e.g. Peate et al., 1997). Mantle xenoliths (Kamenov et al., 2008) also argue for the presence of an Indian-type mantle source beneath the Papuan islands. Derivation from an Indian-type mantle source for the New Caledonian mantle is difficult to ascertain for the lherzolites (see also discussion Secchiari et al., 2018), because these rocks experienced modification of their Sr isotopic signature due to seawater interaction (Secchiari et al., 2016). On the other hand, the strong Pb positive anomalies recorded by whole rock and mineral phases (orthopyroxene and olivine) from the harzburgites support the hypothesis that Pb has been added by a subduction component, which carried the enriched isotopic signature. Hence, the trend in Fig. 8a most likely represents a mixing line relating to mantle contamination by subduction fluids. We thus propose that the Sr–Nd–Pb isotopic signature of the New Caledonia harzburgites are consistent with variable contamination by a subduction component of sedimentary origin at the expense of a depleted MORB type mantle reservoir. Mantle contamination may have occurred both as result of fluid influx from the subducted slab and through subsequent interaction with subduction-related melts carrying a component of sedimentary origin (e.g. the gabbronorite-forming melts from the New Caledonia intrusive sequence; Secchiari et al., 2018).

6. Summary and conclusions

In this work a comprehensive petrological, geochemical and isotopic characterization of the New Caledonia harzburgites has been carried out. Our work allowed to track the history of this mantle section, starting from melting towards late-stage metasomatic evolution (Fig. 13).

The New Caledonia harzburgites are refractory mantle residues, whose main mineralogical and geochemical features (i.e. mineral mode, whole rock and mineral major element compositions, HREE contents) can be explained by extremely high melting degrees of a

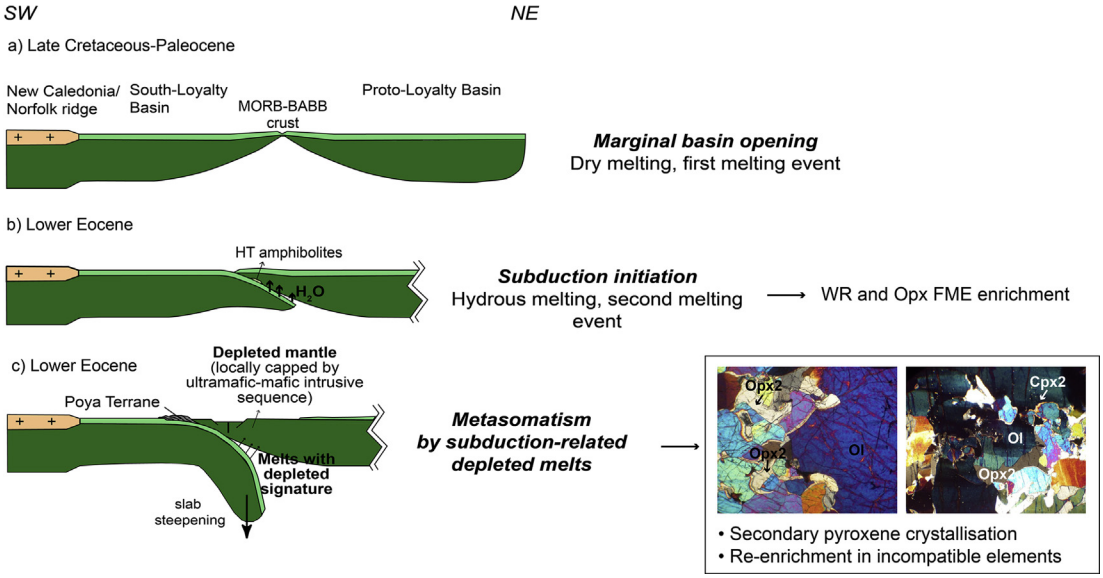

Fig. 13. Schematic sketch model representing the evolution of the New Caledonia harzburgite from late Cretaceous to Eocene (modified after Cluzel et al., 2001). (a) Marginal basin formation (late Cretaceous-Paleocene) and first melting event (dry melting); (b) convergence and subduction initiation (lower Eocene). Dehydration of the lower plate caused fluid ascent towards the upper plate and hydrous melting (second melting event), with concomitant whole rock and orthopyroxene FME enrichment; (c) the refractory harzburgite experiences metasomatism due to interaction with depleted melts bearing a subduction zone signature. Metasomatism is marked by secondary pyroxenes precipitation (Opx2 and Cpx2) together with whole rock and orthopyroxene re-enrichment in incompatible trace elements (i.e. LREE and MREE, HFSE).

depleted mantle source in the spinel stability field. Melting likely occurred in two different stages, i.e. a first melting event under anhydrous conditions (Fig. 13a), followed by fluid-asssisted melting in a subduction zone setting (Fig. 13b).

The enrichment in FME (i.e. Ba, Sr, Pb), LREE–MREE and Nb, Zr, Hf, coupled with the presence of secondary interstitial phases, may be explained by syn- and post-melting interactions with different subduction-related components, possibly aqueous fluids and melts with a depleted trace element signature originated in the forearc setting (Fig. 13c). Nd and Pb isotopic compositions, ranging from DMM values towards enriched, sediment-like isotopic signatures, support a derivation from a DMM reservoir variably contaminated by slab-derived fluids.

We propose that the polyphase evolution recorded by the New Caledonia harzburgites was likely related to seafloor spreading in a marginal basin (late Cretaceous-Paleocene) and subsequent involvement in the Eocene subduction system.

Acknowledgements

The authors are grateful to B. Galland, C. Douchet, O. Bruguier, P. Verdoux and P. Telouk for their expertise in chemical room management, ICP-MS, TIMS and MC-ICP-MS analyses, respectively. We would like to thank Daniele Brunelli (University of Modena) and Roberto Braga (University of Bologna) for providing access to XRF analyses. We also thank E. Saccani for editorial handling. Constructive reviews by Michel Gregoire and Tomoaki Morishita are gratefully acknowledged. This paper is part of the PhD work of A.S., which was supported by a Vinci grant (Italian–French University) and by Italian-PRIN prot. 2015C5LN35.

Appendix A. Supplementary data

Supplementary data to this article can be found online at https://doi.org/10.1016/j.gsf.2019.04.004.

References

Aitchison, J.C., Clarke, L., Meffre, S., Cluzel, D., 1995. Eocene arc-continent collision in New Caledonia and implications for regional Southwest Pacific tectonic evolution. Geology 23, 161–164.

Arai, S., 1994. Characterization of spinel peridotites by olivine-spinel compositional relationships: review and interpretation. Chemical Geology 113, 191–204.

Arai, S., 2004. Petrology of peridotite xenoliths from Iraya volcano, Philippines, and its implication for dynamic mantle-wedge processes. Journal of Petrology 45, 369–389.

Arai, S., Ishimaru, S., 2008. Insights into petrological characteristics of the lithosphere of mantle wedge beneath arcs through peridotite xenoliths: a review. Journal of Petrology 49, 665–695.

Arai, S., Ishimaru, S., Okrugin, V.M., 2003. Metasomatised hazburgite xenoliths from Avacha volcano as fragments of mantle wedge of the Kamchatka arc: implication for the metasomatic agent. Island Arc 12, 233–246.

Arai, S., Takada, S., Michibayashi, K., Kida, M., 2004. Petrology of peridotite xenoliths from Iraya volcano, Philippines, and its implications for dynamic mantle-wedge processes. Journal of Petrology 45, 369–389.

Avias, J., 1967. Overthrust structure of the main ultrabasic New Caledonian massives. Tectonophysics 4, 531–541.

Bizimis, M., Salters, V.J.M., Bonatti, E., 2000. Trace and REE content of clinopyroxenes from supra-subduction zone peridotites. Implications for melting and enrichment processes in island arcs. Chemical Geology 165, 67–85.

Bodinier, J.-L., Godard, M., 2014. Orogenic, Ophiolitic, and Abyssal Peridotites, third ed. Treatise on Geochemistry Elsevier Ltd, pp. 103–170.

Blake Jr., M.C., Brothers, R.N., Lanphere, M.A., 1977. Radiometric ages of blueschists in New Caledonia. In: International Symposium on Geodynamics of the South-West Pacific, Nouméa, vol. 1976, pp. 279–282. Technip.

Brenan, J.M., Shaw, H.F., Ryerson, F.J., Phinney, D.L., 1995. Experimental determination of trace-element partitioning between pargasite and a synthetic hydrous andesitic melt. Earth and Planetary Science Letters 135, 1–11.

Brey, G.P., Kohler, T., 1990. Geothermobarometry in four-phase lherzolites II. New thermobarometers, and practical assessment of existing thermobarometers. Journal of Petrology 31, 1353–1378.

Brounce, M., Kelley, K.A., Cottrell, E., Reagan, M.K., 2015. Temporal evolution of mantle wedge oxygen fugacity during subduction initiation. Geology 43, 775–778.

Chauvel, C., Blichert-Toft, J., 2001. A hafnium isotope and trace element perspective on melting of the depleted mantle. Earth and Planetary Science Letters 190, 137–151.

Cipriani, A., Brueckner, H.K., Bonatti, E., Brunelli, D., 2004. Oceanic crust generated by elusive parents: Sr and Nd isotopes in basalt-peridotite pairs from the Mid-Atlantic ridge. Geology 32, 657–660.

Cluzel, D., Chiron, D., Courme, M.D., 1998. Discordance de l'Eocène supérieur et événements pré-obduction en Nouvelle-Calédonie (Pacifique Sud-Ouest). Comptes rendus l'Académie des Sciences Série 2 Sci de la Terre et des Planetes 327, 485–491 (in France with English abstract).

Cluzel, D., Aitchison, J.C., Picard, C., 2001. Tectonic accretion and underplating of mafic terranes in the Late Eocene intraoceanic forearc of New Caledonia (Southwest Pacific): geodynamic implications. Tectonophysics 340, 23–59.

Cluzel, D., Jourdan, F., Meffre, S., Maurizot, P., Lesimple, S., 2012a. The metamorphic sole of New Caledonia ophiolite: $^{40}Ar/^{39}Ar$, U-Pb, and geochemical evidence for subduction inception at a spreading ridge. Tectonics 31, TC3016. https://doi.org/10.1029/2011TC003085.

Cluzel, D., Maurizot, P., Collot, J., Sevin, B., 2012b. An outline of the Geology of New Caledonia; from Permian – Mesozoic Southeast Gondwanaland active margin to Cenozoic obduction and supergene evolution. Episodes 35, 72–86.

Cluzel, D., Meffre, S., Maurizot, P., Crawford, A.J., 2006. Earliest Eocene (53 Ma) convergence in the Southwest Pacific; evidence from pre-obduction dikes in the ophiolite of New Caledonia. Terra Nova 18, 395–402.

Cluzel, D., Ulrich, M., Jourdan, F., Meffre, S., Paquette, J.L., Audet, M.A., Secchiari, A., Maurizot, P., 2016. Early Eocene clinoenstatite boninite and boninite-series dikes of the ophiolite of New Caledonia; a witness of slab-derived enrichment of the mantle wedge in a nascent volcanic arc. Lithos 260, 429–442.

Coogan, L.A., Thompson, G.M., MacLeod, C.J., 2002. A textural and geochemical investigation of high level gabbros from the Oman ophiolite: implications for the role of the axial magma chamber at fast-spreading ridges. Lithos 63, 67–82.

Collot, J.Y., Malahoff, A., Recy, J., Latham, G., Missegue, F., 1987. Overthrust emplacement of New Caledonia ophiolite: Geophysical evidence. Tectonics 6, 215–232.

De Hoog, J.C.M., Gall, L., Cornell, D.H., 2010. Trace-element geochemistry of mantle olivine and application to mantle petrogenesis and geothermobarometry. Chemical Geology 270, 196–215.

Dhuime, B., Bosch, D., Bodinier, J.L., Garrido, C.J., Bruguier, O., Hussain, S.S., Dawood, H., 2007. Multistage evolution of the Jijal ultramafic–mafic complex (Kohistan, N Pakistan): implications for building the roots of island arcs. Earth and Planetary Science Letters 261, 179–200.

Dick, H.J.B., Bullen, T., 1984. Chromian spinel as a petrogenetic indicator in abyssal and alpine-type peridotites and spatially associated lavas. Contributions to Mineralogy and Petrology 86, 54–76.

Dupuy, C., Dostal, J., Leblanc, M., 1981. Geochemistry of an ophiolitic complex from New Caledonia. Contributions to Mineralogy and Petrology 76, 77–83.

Eisele, J., Sharma, M., Galer, S.J.G., Blichert-Toft, J., Devey, C.W., Hofmann, A.W., 2002. The role of sediment recycling in EM-1 inferred from Os, Pb, Hf, Nd, Sr isotope and trace element systematics of the Pitcairn hotspot. Earth and Planetary Science Letters 196, 197–212.

Eissen, J.-P., Crawford, A.J., Cotten, J., Meffre, S., Bellon, H., Delaune, M., 1998. Geochemistry and tectonic significance of basalts in the Poya Terrane, New Caledonia. Tectonophysics 284, 203–219.

Elliott, T., Plank, T., Zindler, A., White, W., Bourdon, B., 1997. Element transport from slab to volcanic front at the Mariana arc. Journal of Geophysical Research 102, 14991–15019.

Gaetani, G.A., Grove, T.L., 1998. The influence of water on melting of mantle peridotite. Contributions to Mineralogy and Petrology 131, 323–346.

Grégoire, M., McInnes, B.I., O'Reilly, S.Y., 2001. Hydrous metasomatism of oceanic sub-arc mantle, Lihir, Papua New Guinea: Part 2. Trace element characteristics of slab-derived fluids. Lithos 59, 91–108.

Gregoire, M., Jego, S., Maury, R.C., Polve, M., Payot, B., Tamayo Jr., R.A., Yumul Jr., G.P., 2008. Metasomatic interactions between slab-derived melts and depleted mantle: insights from xenoliths within Monglo adakite (Luzon arc, Philippines). Lithos 103, 415–430.

Harvey, J., Gannoun, A., Burton, K.W., Rogers, N.W., Alard, O., Parkinson, I.J., 2006. Ancient melt extraction from the oceanic upper mantle revealed by Re – Os isotopes in abyssal peridotites from the Mid-Atlantic ridge. Earth and Planetary Science Letters 244, 606–621.

Hawthorne, F.C., Oberti, R., Harlow, G.E., Maresch, W.V., Martin, R.F., Schumacher, J.C., Welch, M.D., 2012. Nomenclature of the amphibole supergroup. American Mineralogist 97, 2031–2048.

Hemming, S.R., McLennan, S.M., 2001. Pb-isotope composition of modern deep sea turbidites. Earth and Planetary Science Letters 184, 489–503.

Herzberg, C., 2004. Geodynamic information in peridotite petrology. Journal of Petrology 45, 2507–2530.

Hickey-Vargas, R., Hergt, J.M., Spadea, P., 1995. The Indian Ocean-type isotopic signature in Western Pacific marginal basins: origin and significance. In: Taylor, B., Natland, J. (Eds.), Active Margins and Marginal Basins of Western Pacific. AGU, Washington, D. C, pp. 175–197.

Hirschmann, M.M., Asimow, P.D., Ghiorso, M.S., Stolper, E.M., 1999. Calculation of peridotite partial melting from thermodynamic models of minerals and melts.

III. Controls on Isobaric melt production and the effect of water on melt production. Journal of Petrology 40, 831–851.
Hofmann, A.W., 2003. Sampling mantle heterogeneity through oceanic basalts: isotopes and trace elements. In: Carlson, R.W., Holland, H.D., Turekian, K.K. (Eds.), Treatise on Geochemistry: The Mantle and Core. Elsevier, New York, pp. 61–101.
Ionov, D.A., Savoyant, L., Dupuy, C., 1992. Application of the ICP-MS technique to trace element analysis of peridotites and their minerals. Geostandard newsletters 16, 311–315.
Ionov, D.A., Bodinier, J.-L., Mukasa, S.B., Zanetti, A., 2002. Mechanisms and sources of mantle metasomatism: major and trace element compositions of peridotite xenoliths from spitsbergen in the context of numerical modelling. Journal of Petrology 43, 2219–2259.
Ishii, T., Robinson, P.T., Maekawa, H., Fiske, R., 1992. Petrological studies of peridotites from diapiric serpentinite seamounts in the Izu-Ogasawara-mariana forearc, leg 125. Proceedings ocean drilling program. Scientific Results 125, 445–485.
Ishimaru, S., Arai, S., Ishida, Y., Shirasaka, M., Okrugin, V.M., 2007. Melting and multi-stage metasomatism in the mantle wedge beneath a frontal arc inferred from highly depleted peridotite xenoliths from the Avacha volcano, southern Kamchatka. Journal of Petrology 48, 395–433.
Ishizuka, O., Tani, K., Reagan, M.K., Kanayama, K., Umino, S., Harigane, Y., Sakamoto, I., Miyajima, Y., Yuasa, M., Dunkley, D.J., 2011. The timescales of subduction initiation and subsequent evolution of an oceanic island arc. Earth and Planetary Science Letters 306, 229–240.
Ishizuka, O., Taylor, R.N., Milton, J.A., Nesbitt, R.W., 2003. Fluid-mantle interaction in an intra-oceanic arc: constraints from high-precision Pb isotopes. Earth and Planetary Science Letters 211, 221–236.
Jean, M.M., Shervais, J.W., 2017. The distribution of fluid mobile and other incompatible trace elements in orthopyroxene from mantle wedge peridotites. Chemical Geology 457, 118–130.
Kamenov, G.D., Perfit, M.R., Mueller, P.A., Jonasson, I.R., 2008. Controls on magmatism in an island arc environment: study of lavas and sub-arc xenoliths from the Tabar-Lihir-Tanga-Feni island chain, Papua New Guinea. Contributions to Mineralogy and Petrology 155, 635–656.
Klemme, S., 2004. The influence of Cr on the garnet–spinel transition in the Earth's mantle: experiments in the system MgO–Cr_2O_3–SiO_2 and thermodynamic modelling. Lithos 77, 639–644.
König, S., Münker, C., Schuth, S., Luguet, A., Hoffmann, J.E., Kuduon, J., 2010. Boninites as windows into trace element mobility in subduction zones. Geochimica et Cosmochimica Acta 74, 684–704.
Lagabrielle, Y., Chauvet, A., Ulrich, M., Guillot, S., 2013. Passive obduction and gravity-driven emplacement of large ophiolitic sheets: the New Caledonia ophiolite (SW Pacific) as a case study? Bulletin de la Societé Geologique Française 184, 545–556.
Li, Y.B., Kimura, J.I., Machida, S., Ishii, T., Ishiwatari, A., Maruyama, S., Qiu, H.N., Ishikawa, T., Kato, Y., Haraguchi, S., Takahata, N., Hirahara, N., Miyazaki, T., 2013. High-Mg adakite and low-Ca boninite from a Bonin fore-arc seamount: implications for the reaction between slab melts and depleted mantle. Journal of Petrology 54, 1149–1175.
Liu, C.Z., Snow, J.E., Hellebrand, E., Brügmann, G., von der Handt, A., Büchl, A., Hofmann, A.W., 2008. Ancient, highly heterogeneous mantle beneath Gakkel ridge, Arctic Ocean. Nature 452, 311–316.
Mahoney, J.J., Frei, R., Tejada, M.L.G., Mo, X.X., Leat, P.T., NaGler, T.F., 1998. Tracing the Indian ocean mantle domain through time: isotopic results from old west Indian, east Tethyan, and South Pacific seafloor. Journal of Petrology 39, 1285–1306.
Marchesi, C., Garrido, C.J., Godard, M., Belley, F., Ferré, E., 2009. Migration and accumulation of ultra-depleted subduction-related melts in the Massif du Sud ophiolite (New Caledonia). Chemical Geology 266, 171–186.
McDade, P., Blundy, J., Wood, B.J., 2003. Trace element partitioning between mantle wedge peridodite and hydrous MgO-rich melt. American Mineralogist 88, 1825–1831.
McInnes, B.I.A., Gregoire, M., Binns, R.A., Herzig, P.M., Hannington, M.D., 2001. Hydrous metasomatism of oceanic sub-arc mantle, Lihir, Papua New Guinea: petrology and geochemistry of fluid-metasomatised mantle wedge xenoliths. Earth and Planetary Science Letters 188, 169–183.
Mibe, K., Fujii, T., Yasuda, A., 2002. Composition of aqueous fluid coexisting with mantle minerals at high pressure and its bearing on the differentiation of the Earth's mantle. Geochimica et Cosmochimica Acta 66, 2273–2285.
Morishita, T., Arai, S., 2003. Evolution of spinel–pyroxene symplectite in spinel–lherzolites from the Horoman Complex, Japan. Contributions to Mineralogy and Petrology 144, 509–522.
Mysen, B.R.O., Boettcher, A.L., 1975. Melting of a hydrous mantle: II. Geochemistry of crystals and liquids formed by anatexis of mantle peridotite at high pressures and high temperatures as a function of controlled activities of water, hydrogen, and carbon dioxide. Journal of Petrology 16, 549–593.
Nimis, P., Taylor, W.R., 2000. Single clinopyroxene thermobarometry for garnet peridotites. Part I. Calibration and testing of a Cr-in-Cpx barometer and an enstatite-in-Cpx thermometer. Contributions to Mineralogy and Petrology 139, 541–554.
Niu, Y., 2004. Bulk-rock major and trace element compositions of abyssal peridotites: implications for mantle melting, melt extraction and post-melting processes beneath mid-ocean ridges. Journal of Petrology 45, 2423–2458.
Niu, Y.L., 1997. Mantle melting and melt extraction processes beneath ocean ridges: evidence from abyssal peridotites. Journal of Petrology 38, 1047–1074.
Ohara, Y., Ishii, T., 1998. Peridotites from the southern Mariana forearc: heterogeneous fluid supply in mantle wedge. Island Arc 7, 541–558.
Othman, D.B., White, W.M., Patchett, J., 1989. The geochemistry of marine sediments, island arc magma genesis, and crust-mantle recycling. Earth and Planetary Science Letters 94, 1–21.
Parkinson, I.J., Pearce, J.A., 1998. Peridotites from the Izu-Bonin-Mariana forearc (ODP leg 125): evidence for mantle melting and melt-mantle interaction in a supra-subduction zone setting. Journal of Petrology 39, 1577–1618.
Paris, J.P., 1981. Géologie de la Nouvelle-Calédonie. Un essai de synthèse: Bureau de Recherches Géologiques et Minières, Memoirs, vol. 113, 278 pp (in France).
Pearce, N.J., Perkins, W.T., Westgate, J.A., Gorton, M.P., Jackson, S.E., Neal, C.R., Chenery, S.P., 1997. A compilation of new and published major and trace element data for NIST SRM 610 and NIST SRM 612 glass reference materials. Geostandard Newsletters 21, 115–144.
Pearce, J.A., Barker, P.F., Edwards, S.J., Parkinson, I.J., Leat, P.T., 2000. Geochemistry and tectonic significance of peridotites from the South Sandwich arc-basin system, South Atlantic. Contributions to Mineralogy and Petrology 139, 36–53.
Peate, D.W., Pearce, J.A., Hawkesworth, C.J., Colley, H., Edwards, C.M.H., Hirose, K., 1997. Geochemical variations in Vanuatu arc lavas: the role of subducted material and a variable mantle wedge composition. Journal of Petrology 38, 1331–1358.
Piccardo, G.B., Zanetti, A., Müntener, O., 2007. Melt/peridotite interaction in the Southern Lanzo peridotite: field, textural and geochemical evidence. Lithos 94, 181–209.
Pin, C., Briot, D., Bassin, C., Poitrasson, F., 1994. Concomitant separation of strontium and samarium–neodymium for isotopic analysis in silicate samples, based on specific extraction chromatography. Analytica Chimica Acta 298, 209–217.
Pirard, C., Hermann, J., O'Neill, H.S.C., 2013. Petrology and geochemistry of the crust-mantle boundary in a Nascent arc, massif du Sud ophiolite, New Caledonia, SW Pacific. Journal of Petrology 54, 1759–1792.
Plank, T., 2013. The Chemical Composition of Subducting Sediments. Treatise on Geochemistry: Second Edition., second ed. Elsevier Ltd., pp. 607–629
Plank, T., Langmuir, C.H., 1998. The chemical composition of subducting sediment and its consequences for the crust and mantle. Chemical Geology 145, 325–394.
Prinzhofer, A., Allègre, C., 1985. Residual peridotites and the mechanisms of partial melting. Earth and Planetary Science Letters 74, 251–265.
Prinzhofer, A., Nicolas, A., Cassard, D., Moutte, J., Leblanc, M., Paris, J.P., Rabinovitch, M., 1980. Structures in the New Caledonia peridotites-gabbros: implications for oceanic mantle and crust. Tectonophysics 69, 85–112.
Prouteau, G., Scaillet, B., Pichavant, M., Maury, R., 2001. Evidence for mantle metasomatism by hydrous silicic melts derived from subducted oceanic crust. Letters To Nature 410, 197–200.
Quesnel, B., Gautier, P., Cathelineau, M., Boulvais, P., Couteau, C., Drouillet, M., 2016. The internal deformation of the Peridotite Nappe of New Caledonia: a structural study of serpentine-bearing faults and shear zones in the Koniambo Massif. Journal of Structural Geology 85, 51–67.
Rampone, E., Piccardo, G.B., Hofmann, A.W., 2008. Multi-stage melt-rock interaction in the Mt. Maggiore (Corsica, France) ophiolitic peridotites: microstructural and geochemical evidence. Contributions to Mineralogy and Petrology 156, 453–475.
Reagan, M.K., Ishizuka, O., Stern, R.J., Kelley, K.A., Ohara, Y., Blichert-Toft, J., Bloomer, S.H., Cash, J., Fryer, P., Hanan, B.B., Hickey-Vargas, R., Ishii, T., Kimura, J.-I., Peate, D.W., Rowe, M.C., Woods, M., 2010. Forearc basalts and subduction initiation in the Izu-Bonin-Mariana system. Geochemistry, Geophysics Geosystems 11, 3.
Salters, V.J.M., Stracke, A., 2004. Composition of the depleted mantle. Geochemistry, Geophysics, Geosystems 5, 5.
Salters, V.J.M., Dick, H.J.B., 2002. Mineralogy of the mid-ocean-ridge basalt source from neodymium isotopic composition of abyssal peridotites. Nature 418, 68–72.
Schuth, S., König, S., Münker, C., 2011. Subduction zone dynamics in the SW Pacific plate boundary region constrained from high-precision Pb isotope data. Earth and Planetary Science Letters 311, 328–338.
Schuth, S., Rohrbach, A., Münker, C., Ballhaus, C., Garbe-Schönberg, D., Qopoto, C., 2004. Geochemical constraints on the petrogenesis of arc picrites and basalts, New Georgia Group, Solomon Islands. Contributions to Mineralogy and Petrology 148, 288–304.
Scott, J.M., Liu, J., Pearson, D.G., Waight, T.E., 2016. Mantle depletion and metasomatism recorded in orthopyroxene in highly depleted peridotites. Chemical Geology 441, 280–291.
Secchiari, A., Montanini, A., Bosch, D., Macera, P., Cluzel, D., 2018. The contrasting geochemical message from the New Caledonia gabbronorites: insights on depletion and contamination processes of the sub-arc mantle in a nascent arc setting. Contributions to Mineralogy and Petrology 173, 66.
Secchiari, A., Montanini, A., Bosch, D., Macera, P., Cluzel, D., 2016. Melt extraction and enrichment processes in the New Caledonia lherzolites : evidence from geochemical and Sr − Nd isotope data. Lithos 260, 28–43.
Secchiari, A., Montanini, A., Bosch, D., Macera, P., Cluzel, D., 2019. Origin of the spinel-pyroxene symplectites in the harzburgites from the New Caledonia peridotite. Ofioliti 44 (1), 31–42.
Seyler, M., Lorand, J.-P., Dick, H.J.B., Drouin, M., 2007. Pervasive melt percolation reactions in ultra-depleted refractory harzburgites at the Mid-Atlantic Ridge, 15° 20′N: ODP Hole 1274A. Contributions to Mineralogy and Petrology 153, 303–319.

Shaw, D.M., 1970. Trace element fractionation during anatexis. Geochimica et Cosmochimica Acta 34, 237–243.
Shervais, J.W., Jean, M.M., 2012. Inside the subduction factory: modeling fluid mobile element enrichment in the mantle wedge above a subduction zone. Geochimica et Cosmochimica Acta 95, 270–285.
Snow, J.E., Dick, H.J.B., 1995. Pervasive magnesium loss by marine weathering of peridotite. Geochimica et Cosmochimica Acta 59, 4219–4235.
Soret, M., Agard, P., Dubacq, B., Vitale-Brovarone, A., Monié, P., Chauvet, A., Whitechurch, H., Villemant, B., 2016. Strain localization and fluid infiltration in the mantle wedge during subduction initiation: evidence from the base of the New Caledonia ophiolite. Lithos 244, 1–19.
Spandler, C., Rubatto, D., Hermann, J., 2005. Late Cretaceous-Tertiary tectonics of the southwest Pacific: insights from U-Pb sensitive, high resolution ion microprobe (SHRIMP) dating of eclogite facies rocks from New Caledonia. Tectonics 24, TC3003.
Stern, R.J., Reagan, M., Ishizuka, O., Ohara, Y., Whattam, S., 2012. To understand subduction initiation, study forearc crust: to understand forearc crust, study ophiolites. Lithosphere 4, 469–483.
Stolper, E., Newman, S., 1994. The role of water in the petrogenesis of Mariana trough magmas. Earth and Planetary Science Letters 121, 293–325.
Stracke, A., Snow, J.E., Hellebrand, E., von der Handt, A., Bourdon, B., Birbaum, K., Günther, D., 2011. Abyssal peridotite Hf isotopes identify extreme mantle depletion. Earth and Planetary Science Letters 308, 359–368.
Sun, C., Liang, Y., 2014. An assessment of subsolidus re-equilibration on REE distribution among mantle minerals olivine, orthopyroxene, clinopyroxene, and garnet in peridotites. Chemical Geology 372, 80–91.
Sun, S.-S., McDonough, W.F., 1989. Chemical and Isotopic Systematics of Oceanic Basalts: Implications for Mantle Composition and Processes, vol. 42. Geological Society, London. Special Publications, pp. 313–345.
Taylor, W.R., 1998. An experimental test of some geothermometer and geobarometer formulations for upper mantle peridotites with application to the thermobarometry of fertile lherzolite and garnet websterite. Journal of Mineralogy and Geochemistry 381–408.
Ulrich, M., Picard, C., Guillot, S., Chauvel, C., Cluzel, D., Meffre, S., 2010. Multiple melting stages and refertilization as indicators for ridge to subduction formation: the New Caledonia ophiolite. Lithos 115, 223–236.
Vernières, J., Godard, M., Bodinier, J.-L., 1997. A plate model for the simulation of trace element fractionation during partial melting and magma transport in the Earth's upper mantle. Journal of Geophysical Research: Solid Earth 102, 24771–24784.
Warren, J.M., Shimizu, N., Sakaguchi, C., Dick, H.J.B., Nakamura, E., 2009. An assessment of upper mantle heterogeneity based on abyssal peridotite isotopic compositions. Journal of Geophysical Research 114, B12203.
Warren, J.M., Shirey, S.B., 2012. Lead and osmium isotopic constraints on the oceanic mantle from single abyssal peridotite sulfides. Earth and Planetary Science Letters 359–360, 279–293.
Webb, S.A.C., Wood, W.J., 1986. Spinel–pyroxene–garnet relationships and their dependence on Cr/Al ratio. Contributions to Mineralogy and Petrology 92, 471–480.
Workman, R.K., Hart, S.R., 2005. Major and trace element composition of the depleted MORB mantle (DMM). Earth and Planetary Science Letters 231, 53–72.
Zanetti, A., D'Antonio, M., Spadea, P., Raffone, N., Vannucci, R., Brugier, O., 2006. Petrogenesis of mantle peridotites from the Izu-Bonin-mariana (IBM) forearc. Ofioliti 31, 189–206.
Zindler, A., Hart, S.R., 1986. Chemical geodynamics. Annual Review of Earth and Planetary Sciences 14, 493–571.